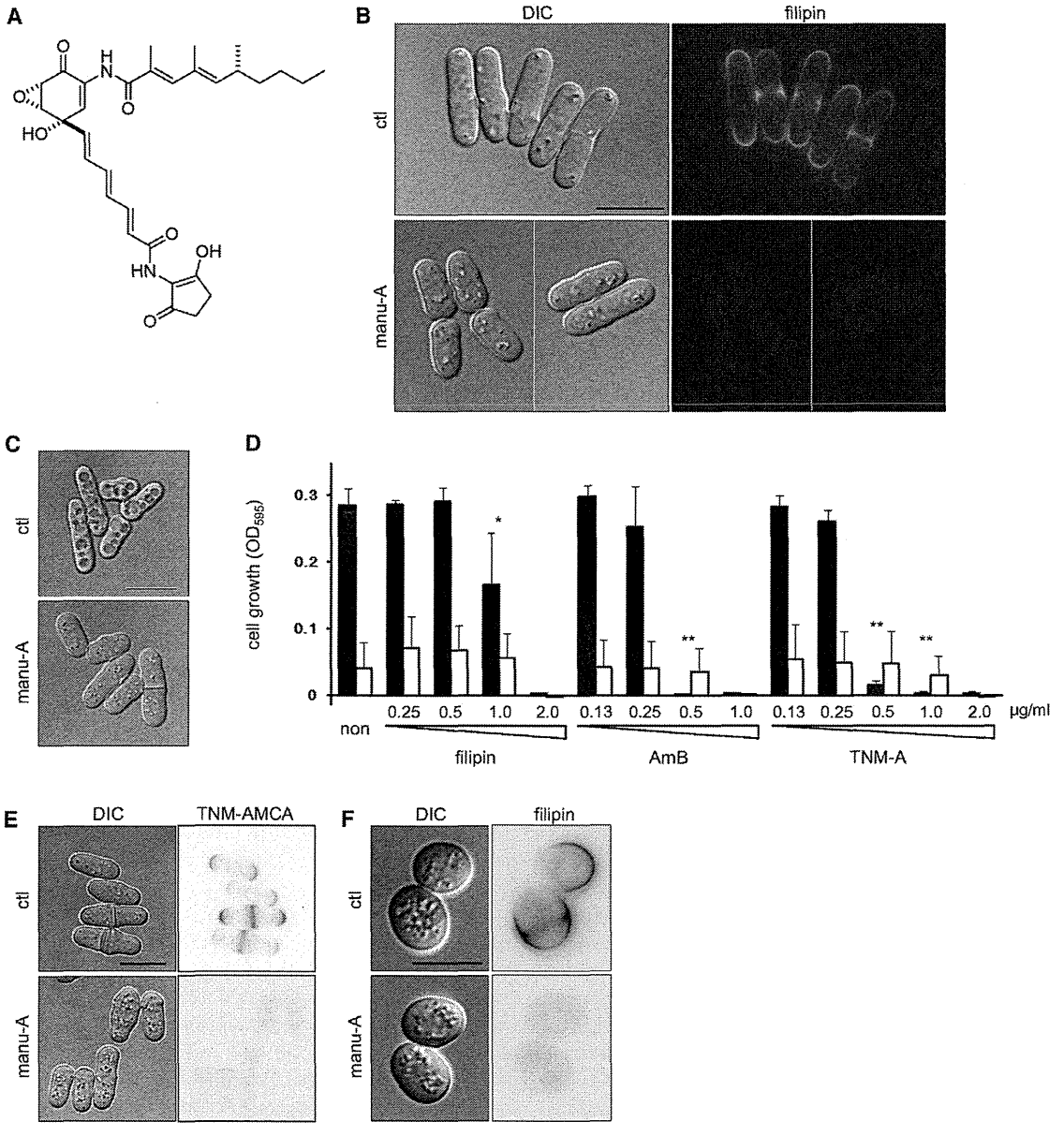

Figure 1. Manu-A Abolishment of the Binding and Effect of Sterol-Binding Antibiotics

(A) Chemical structure of manu-A.

(B) Sterol-rich plasma membrane domains of fission yeast cells. Domains were visualized with filipin (upper right hand panel). Manu-A treatment (1 μg/ml) for 1 hr abolished the fluorescent signal of filipin binding (lower right hand panel).

(C) Cellular effect of AmB. Cells were treated with AmB (1 μg/ml) for 1 hr in the presence or absence of manu-A (1 μg/ml) and observed under microscopy.

(D) Effect of manu-A on the growth inhibition exerted by antibiotics. Yeast cells were incubated with sterol-targeting antibiotics in the presence (white) or absence (black) of manu-A (0.5 μg/ml) for 26 hr. Data represent the mean ± SD, n = 3–4. Statistical significance of $p < 0.05$ (*) and $p < 0.01$ (**) were determined by t test, calculated using cell growth values normalized using optical density of the cultures in the absence of manu-A.

(E) Binding of TNM-AMCA in the presence of manu-A. Cells were incubated with or without manu-A (1 μg/ml) for 1 hr, and then stained with TNM-AMCA (1 μg/ml) for 1 hr.

(F) Sterol-rich domains in *cpp1*Δ cells. The domains were visualized with filipin in the presence or absence of manu-A (1 μg/ml). Scale bars, 10 μm. Control (ctl), differential interference contrast microscopy (DIC).

Relationship between Manu-A and Cdc42

Sterol localization is controlled in a cell cycle-dependent manner (Wachtler et al., 2003); we therefore hypothesized that the effect of manu-A on the plasma membrane would correlate with its cell growth inhibitory activity. To identify the genes involved in the action of manu-A, we conducted a genome-wide screen using a decreased abundance by mRNA perturbation (DAmP) strain collection of the budding yeast *Saccharomyces cerevisiae* (Breslow et al., 2008; Yan et al., 2008). DAmP acts by destabilizing mRNA transcripts through the integration of an

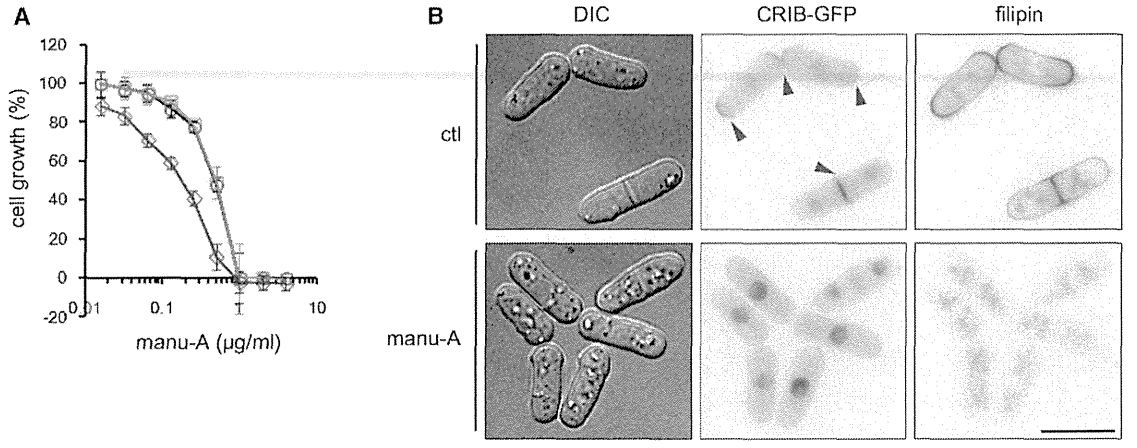

Figure 2. Relationship between Cdc42 and Manu-A

(A) Effect of Cdc42 expression levels on manu-A sensitivity. Cells containing mock vectors (black), cells overexpressing wild-type Cdc42 (blue), or the dominant-negative form, Cdc42-T17N (red), were cultured in the presence of manu-A. Cell growth was measured after 48 hr incubation. Data represent the mean ± SD, n = 4.

(B) Cellular localization of activated Cdc42 (detected using CRIB-GFP) and sterol-rich membrane domains (detected using filipin). Cells treated with or without manu-A (1 μg/ml) for 1 hr were observed under fluorescent microscopy. Arrowheads indicate the colocalization of CRIB-GFP and filipin signals. Scale bar, 10 μm.

antibiotic-selectable marker into the 3′ untranslated regions of genes of interest, thereby yielding hypomorphic alleles (Muhlrad and Parker, 1999). Genes involved in the mode of action of a bioactive compound can then be identified by screening DAmP strain collections for strains that are sensitive to the compound (Breslow et al., 2008; Yan et al., 2008).

The growth of the budding yeast cells was observed to be sensitive to manu-A (Figure S4A). After screening 878 haploid DAmP strains, we identified 28 genes for which downregulation conferred increased sensitivity to manu-A (Figures S4A–S4C). Among these, we found several genes involved in membrane trafficking: *SEC31*, which encodes a component of the COPII vesicle coat required for vesicle formation in ER-to-Golgi transport; and *PAN1*, which encodes a protein that associates with actin patches and promotes protein-protein interactions essential for endocytosis. *ERG8*, an essential gene for the biosynthesis of isoprenoids and ergosterol, was also identified. Notably, *CDC24*, which encodes a guanosine diphosphate-guanosine triphosphate (GTP) exchange factor for Cdc42, was similarly identified as a sensitive DAmP mutant (Park and Bi, 2007). Cdc42 is known to regulate the polarization of the actin cytoskeleton and membrane trafficking toward the sites of cell growth (Park and Bi, 2007; Perez and Rincón, 2010).

These results led us to hypothesize that manu-A perturbs Cdc42, which in turn effects the formation of sterol-rich membrane domains. To test whether manu-A targets the Cdc42 pathway in fission yeast, we first examined the effect of overexpression of Cdc42 on the growth inhibitory activity of manu-A. Overexpression of wild-type Cdc42 had no effect, whereas cells expressing the dominant-negative form of Cdc42 became more sensitive to manu-A compared with cells containing mock vectors (Figure 2A). We next examined the activity of Cdc42 using a fluorescent fusion protein called Cdc42/Rac interactive binding peptide-green fluorescent protein (CRIB)-GFP, which specifically binds to activated, GTP-bound Cdc42 (Tatebe et al., 2008). In wild-type cells, CRIB-GFP signal was concentrated at the growing cell tips during interphase and around the division plane during mitosis (Figure 2B). After the addition of manu-A, cortical GFP signal was barely detectable, indicating that Cdc42 was inactivated. In contrast, cortical localization visualized using GFP-Cdc42 fusion protein was not abolished completely, and the prenylation status of Cdc42 protein appeared unaffected by manu-A (Figures S4D and S4E). Together, these results suggested that the Cdc42 activation pathway is targeted by manu-A in fission yeast cells.

Inhibition of Exocytosis by Manu-A

In fission yeast cells, Cdc42 regulates the actin cytoskeleton (Martin et al., 2007; Rincón et al., 2009) and multiple membrane trafficking events (Estravís et al., 2011). Since Cdc42 was downregulated by manu-A, we next investigated whether the effect of manu-A was mediated through the disorganization of the actin cytoskeleton and/or dysregulation of membrane trafficking. In fission yeast cells, the actin cytoskeleton consists of actin cables, actin patches, and a contractile ring during vegetative growth (Kovar et al., 2011). Cells treated with manu-A exhibited apparently delocalized actin patches with randomly localized actin cables, indicating that cells lost polarity in actin structures in the presence of manu-A (Figure S5A). However, genetic perturbation of the actin cytoskeleton organization did not result in a similar phenotype; when temperature-sensitive *cps8-188* cells were left at the restriction temperature, the fluorescent signal of filipin became delocalized and distributed over the plasma membrane (Codlin et al., 2008). Furthermore, the effect of manu-A on cell growth was almost indistinguishable between actin mutant cells and wild-type cells (Figure 3A). These results indicated that the effect of manu-A on the plasma membrane was not exerted through disorganization of the actin cytoskeleton.

Next, we investigated the relationship between manu-A and membrane trafficking. A terminal phenotype of a thermosensitive

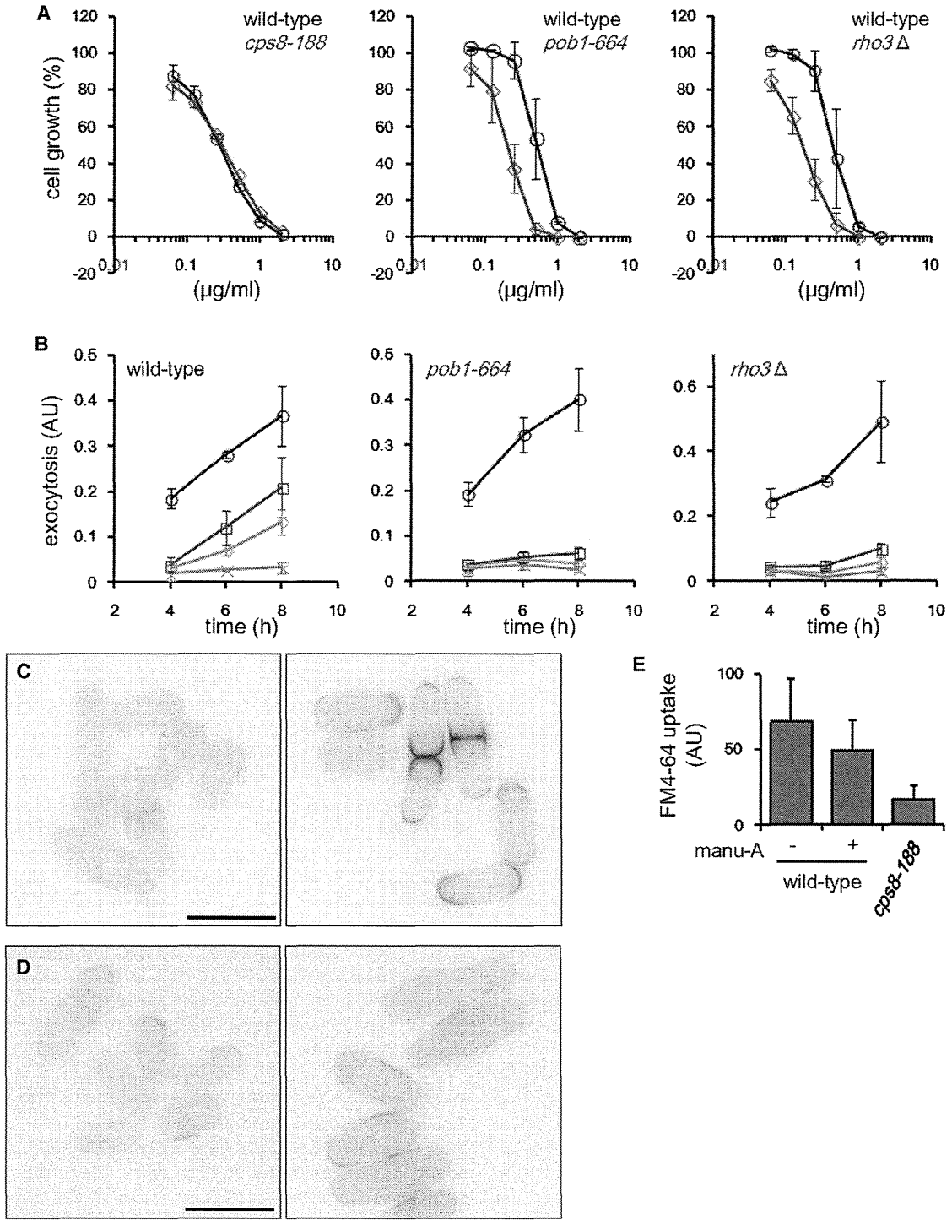

Figure 3. Effect of Manu-A on Cell Growth, Exocytosis, and Endocytosis

(A) Growth inhibition of mutant cells by manu-A. Growth of *cps8-188* cells (27°C for 24 hr), *pob1-664* cells (30°C for 26 hr), and *rho3*Δ cells (30°C for 26 hr) in the presence of manu-A was compared with that of wild-type cells.

(B) Exocytosis inhibition by manu-A. Activity of secreted acid phosphatase from wild-type, *pob1* mutant, and *rho3* deletion cells in the presence of manu-A was measured. Acid phosphatase activity was normalized with cell density. Cells were cultivated at 27°C and at various manu-A concentrations: 0 (black), 0.05 (red), 0.1 (blue), and 0.5 (green) μg/ml.

(C) Reappearance of sterol-rich membrane domains after treatment with a low concentration of manu-A. Manu-A (0.05 μg/ml) was added to the cells in EMMP, followed by visualization of sterol-rich membrane domains using filipin. Fluorescent images after 1 hr treatment (left) and 5 hr treatment (right) are shown.

(legend continued on next page)

strain of *cdc42* is a defect in exocytosis (Estravís et al., 2011). To test the possibility that manu-A inhibits exocytosis, we measured the secretion of acid phosphatase, a protein marker of exocytosis (Wang et al., 2002). When cells were exposed to manu-A, secretion of acid phosphatase was inhibited in a dose-dependent manner (Figure 3B). The effective concentration was comparable to that necessary for inhibiting the cellular binding of antibiotics. Many protein factors have been reported to be involved in exocytosis; for example, Pob1, which is involved in polarized growth; and a small GTPase, Rho3, which regulates cell separation. Although the precise molecular mechanism remains to be clarified, introducing mutations in the *pob1* gene (*pob1-664*; see Nakano et al., 2011) or deletion of the *rho3* gene (*rho3*Δ; see Wang et al., 2003) have been shown to decrease secretion resulting from exocytosis. When we challenged these mutant cells with manu-A, exocytosis was suppressed at lower manu-A concentrations compared with the wild-type cells (Figure 3B); moderate inhibition was observed in wild-type cells at 0.05–0.1 μg/ml, whereas exocytosis was almost completely inhibited in the mutant cells at a concentration as low as 0.05 μg/ml. Additionally, manu-A more efficiently inhibited cell growth of the exocytosis mutant cells compared with the wild-type cells (Figure 3A). In contrast, exocytosis of actin mutant cells was not more sensitive to manu-A compared with wild-type cells (Figure S5B). These results showed that the observed cell growth inhibition by manu-A was, at least in part, a result of the suppression of exocytosis, which in turn led to the loss of cellular binding of sterol-targeting antibiotics.

Inhibition of Exocytosis Leads to the Disappearance of Sterol-Rich Plasma Membrane Domains

Treatment of wild-type cells with manu-A at a low concentration (0.05 μg/ml) inhibited exocytosis, but this inhibition was gradually released (Figure 3B). If exocytosis supplies sterol-rich membrane domains, recovery of exocytosis should lead to the recovery of these membrane domains. We indeed observed this using filipin staining of cells treated with a low concentration of manu-A; although treating wild-type cells with 0.05 μg/ml manu-A for 1 hr initially abolished the filipin signal, the same signal reappeared 5 hr later (Figure 3C). In contrast, when higher concentrations of manu-A were used, e.g., 0.5 μg/ml, the filipin signal was only barely detectable 6 hr following the initial treatment (Figure S6).

The exocytosis activities of the *pob1* mutant and *rho3*Δ cells were found to be more sensitive to manu-A than that of wild-type cells. We examined recovery of the filipin signal in these mutant cells and found that in *pob1* mutant cells, recovery of the filipin signal was not observed (Figure 3D). Similarly, the lack of *rho3* protein significantly perturbed the signal recovery and only weak and irregular filipin staining was observed (Figure 3D). Together, these results indicate that manu-A inhibits exocytosis, the route by which the sterol-rich membrane domains are supplied to the plasma membrane.

Endocytosis Is Requisite for the Disappearance of Sterol-Rich Plasma Membrane Domains

Manu-A inhibits exocytosis, and this inhibition appears to abolish the production of sterol-rich membrane domains in the plasma membrane. However, inhibition of the supply of sterol-rich membrane domains may not to be sufficient for the complete abolishment of antibiotic action, since certain portions of the sterol-rich membrane domains should already have been delivered to the plasma membrane prior to the addition of manu-A. This suggested the possibility that endocytosis could selectively internalize these domains, a process that may not be inhibited by manu-A. Our next experiments therefore tested the effect of manu-A on endocytosis.

In fission yeast cells, the fluorescent styryl dye FM4-64 is used as a marker for the endocytic pathway, as FM4-64 is internalized by endocytosis at the growing areas of the cell and is subsequently transported to the vacuolar membrane (Gachet and Hyams, 2005). Within 30 min of the addition of FM4-64, intermediate compartments became stained despite the presence of manu-A (although the dye intensity was slightly decreased), indicating that endocytosis was uninhibited by manu-A (Figure 3E). This analysis suggested that manu-A did not inhibit the uptake of plasma membrane domains, despite inhibiting the supply thereof to the membrane and consequently inhibiting the generation of sterol-rich membrane domains. This corroborates a previous finding in budding yeast, where secretory vesicles were observed to be enriched in ergosterol and sphingolipids (Klemm et al., 2009).

We also tested the effect of BFA on FM4-64 incorporation. Cells treated with BFA showed intense and nonpolarized filipin signal (Figure S1A). If the balance of exocytosis and endocytosis determines the binding of sterol-targeting antibiotics, BFA should have the opposite effect of manu-A. As expected, BFA suppressed incorporation of FM4-64 (Figure S1C). This was consistent with a previous report demonstrating BFA inhibition of FM4-64 incorporation at the equatorial region in dividing cells (Gachet and Hyams, 2005). In contrast, the secretion of acid phosphatase was unaffected (Figure S1B). This result indicated that the continuing export and simultaneous inhibition of the uptake of membrane domains by BFA led to the accumulation of sterols in the plasma membrane as visualized with filipin staining.

Heat Shock Leads to the Disappearance of Sterol-Rich Plasma Membrane Domains

Heat shock treatment induces a variety of cellular responses to adapt to this condition (Verghese et al., 2012). We found that sterol-rich membrane domains are also sensitive to heat shock, as the filipin signal in wild-type cells was significantly decreased after the temperature was shifted from 27°C to 37°C (Figure 4A). This response was transient and the sterol-rich membrane

(D) Lack of reappearance of sterol-rich membrane domains in mutant cells. *pob1-664* (left) and *rho3*Δ cells (right) were treated with 0.05 μg/ml manu-A and stained with filipin after 5 hr.

(E) Effect of manu-A on endocytosis. Uptake of FM4-64 by wild-type cells was observed after treatment with DMSO (0.1%) or manu-A (1 μg/ml) for 1 hr. FM4-64 was added to the culture and cells were observed under fluorescence microscopy. Uptake of FM4-64 was calculated after 0.5 hr. In a control experiment, *cps8-188* cells were shifted to the restriction temperature (37°C) for 1 hr, followed by FM4-64 treatment and observation of FM4-64 uptake.

In (A) and (B), data represent the mean ± error bars, SD, n = 3. In (E), data represent the mean ± error bars, SE, n = 3.

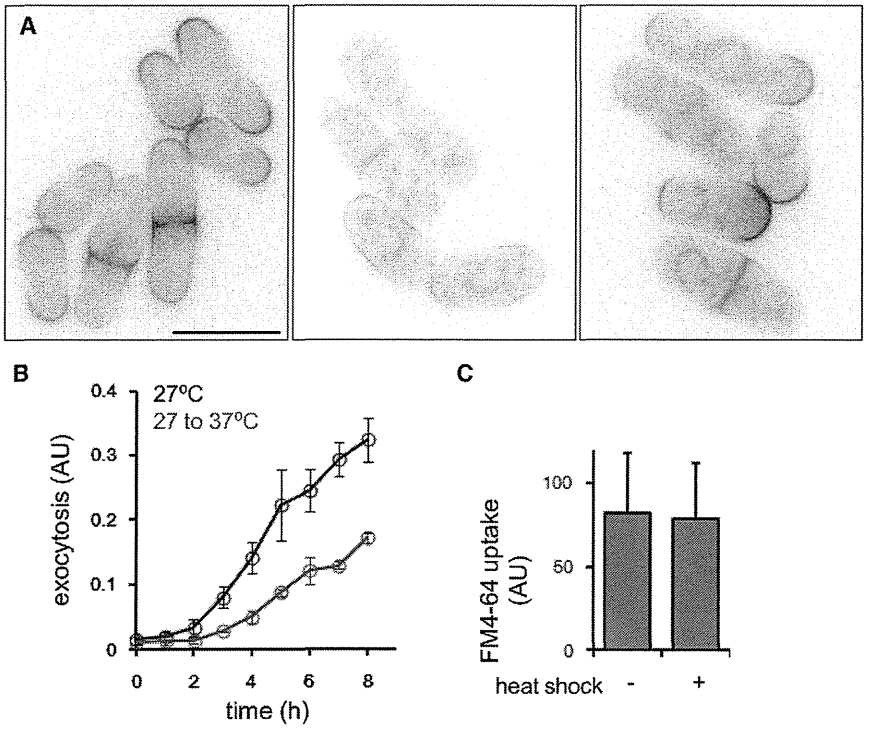

Figure 4. Transient Disappearance of Sterol-Rich Plasma Membrane Domains following Heat Shock

(A) Disappearance and reappearance of sterol-rich plasma membrane domains following heat shock treatment. Wild-type cells in YE5S were shifted from 27°C (left) to 37°C for 1 hr (middle) and 5 hr (right), and the presence of sterol-rich membrane domains was visualized using filipin. Scale bar, 10 μm.

(B) Kinetics of exocytosis after heat shock. Cells were cultured at 27°C (black) or shifted from 27°C to 37°C (red) at time 0. Activity of secreted acid phosphatase was measured and normalized with cell density. Data represent the mean ± SD, n = 3.

(C) Effect of heat shock on endocytosis. Wild-type cells in YE5S were shifted from 27°C (left) to 37°C for 1 hr, and uptake of FM4-64 was observed. Data represent the mean ± SE, n = 3.

domains gradually reappeared (Figure 4A). We hypothesized that this phenomena may be similar in mechanism to that of treatment with low concentrations of manu-A, and we expected that while heat shock may transiently suppress exocytosis, endocytosis would not be affected. To test this hypothesis, we analyzed the kinetics of exocytosis after heat shock (Figure 4B). As expected, exocytosis was attenuated and no release of acid phosphatase was observed 2 hr after the temperature shift. As a consequence, the concentration of released acid phosphatase was lower than that for the control cells (no temperature shift). In contrast, cellular uptake of FM4-64 was uninhibited by the temperature shift (Figure 4C). We therefore concluded that heat shock temporarily halts exocytosis, but not endocytosis, thereby facilitating the disappearance of sterol-rich membrane domains in the plasma membrane, similar in effect to manu-A treatment.

Sterol-Targeting Antibiotic-Resistant Cells Exhibit Defect in Exocytosis

Resistance to antibiotics can be the result of multiple mechanisms. Our emerging model suggested the possibility that cells may exhibit tolerance toward sterol-targeting antibiotics where a defect in exocytosis is present. To investigate this possibility, we first examined the secretion of acid phosphatase from ergosterol mutant cells. Knockout of the *erg2* gene or simultaneous deletion of the *erg31* and *erg32* genes in fission yeast is known to cause tolerance to sterol-targeting antibiotics (Iwaki et al., 2008). However, we could not detect any defects in acid phosphatase secretion (data not shown).

We next examined overexpression of the *SPCC23B6.04c* gene. We previously conducted genome-wide screening to identify genes conferring altered sensitivity to chemicals by their overexpression (Nishimura et al., 2010). Among the ~4,800 genes screened, *SPCC23B6.04c* was identified as a resistance gene common to AmB, nystatin, and TNM-F, a closely related congener of TNM-A (Matsunaga et al., 1989). We first investigated the cellular binding of filipin and TNM-AMCA to cells overexpressing *SPCC23B6.04c*. As expected, neither compound bound to the cells (Figures 5A and 5B), suggesting that antibiotic-sensitive sterol-rich membrane domains are not supplied to the plasma membrane in these cells. Next, we measured the degree of exocytosis and endocytosis. We found that the secretion of acid phosphatase was significantly decreased by overexpression of *SPCC23B6.04c* (Figure 5C). When overexpression was suppressed by addition of thiamine, this defect was not observed. In contrast, endocytosis was unaffected by overexpression of this gene (Figure 5D). The intensity of FM4-64 dye incorporated into these cells was no different to that of the control cells. Although the molecular function of the gene product of *SPCC23B6.04c* is still unknown, these results add further support to our model (discussed below, Figure 6).

Model for the Generation of Antibiotic-Sensitive Sterol-Rich Plasma Membrane Domains

Based on our results, we propose a model in which exocytosis supplies and endocytosis internalizes the specific membrane domains recognized by sterol-targeting antibiotics (Figure 6). In this study, we first showed that manu-A caused defects in membrane trafficking and abolishment of the effect of sterol-targeting antibiotics. Manu-A inhibited Cdc42 activity and its downstream event, exocytosis. In contrast, endocytosis was only partially inhibited. Heat shock and overexpression of a gene with unknown function, *SPCC23B6.04c*, induced similar defects in membrane trafficking and decreased binding of sterol-targeting antibiotics. BFA inhibited the incorporation of FM4-64, but not the secretion of acid phosphatase. Treatment with BFA exhibited intense fluorescence of filipin at the plasma membrane, suggesting that the selective inhibition of endocytosis resulted in the accumulation

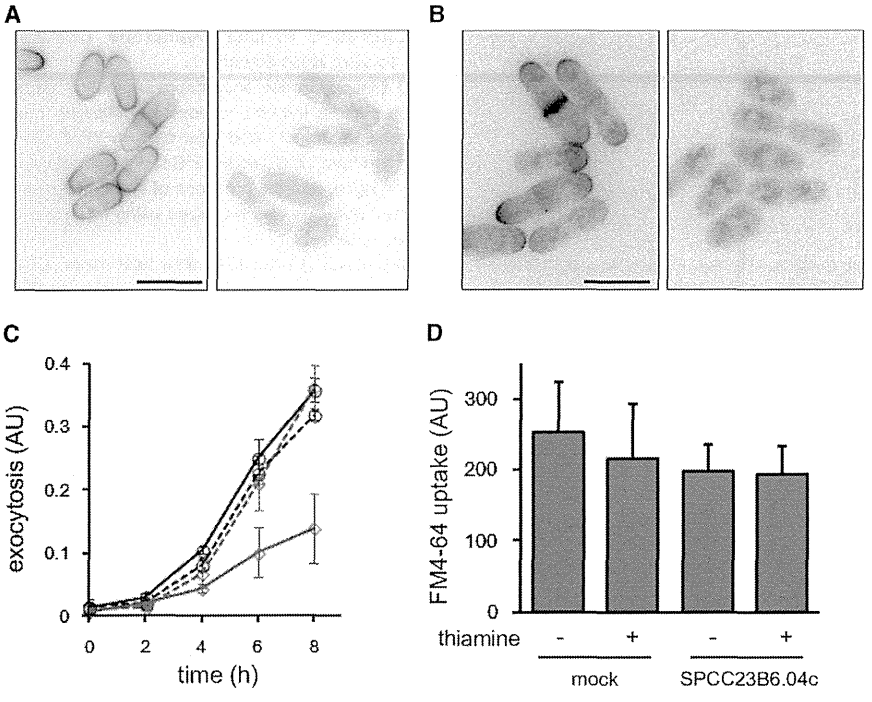

Figure 5. Effect of Overexpression of *SPCC23B6.04c* on Sterol-Targeting Antibiotics and Membrane Trafficking

(A and B) Binding of filipin (A) or TNM-AMCA (B) to control cells (left) and *SPCC23B6.04c*-overexpressing cells (right). Scale bars, 10 μm.

(C) Attenuation of exocytosis by overexpressing *SPCC23B6.04c*. Activity of secreted acid phosphatase from control cells (black) and overexpressing cells (red) in the absence (solid) or presence (dashed) of thiamine was measured. Acid phosphatase activity was normalized with cell density. Cells were cultivated at 27°C. Error bars, SD, n = 3.

(D) Effect of overexpression of *SPCC23B6.04c* on endocytosis. Uptake of FM4-64 by control and overexpressing cells was observed. Error bars, SE, n = 3.

of excess sterols. Taken together, balanced membrane trafficking appears essential for the regulation of the quantity of antibiotic-sensitive and sterol-rich domains in the plasma membrane.

SIGNIFICANCE

The species and quantity of lipid molecules in the plasma membrane are maintained by multiple mechanisms involving vesicle transport, lipid transport proteins, and local metabolic reactions (van Meer et al., 2008). Here, we have demonstrated that the proper balance between exocytosis and endocytosis produces membrane domains that are recognized by sterol-targeting antibiotics, as the specific inhibition of exocytosis, but not endocytosis by manu-A, heat shock, or overexpression of *SPCC23B6.04c*, all abolished the cellular binding of these antibiotics. Originally, membrane domains stainable by filipin were termed sterol-rich membrane domains (Wachtler et al., 2003), and similar staining patterns have since been observed when using fluorescently labeled TNMs (Nishimura et al., 2010). However, manu-A abolished the efficacy of not only filipin and TNMs, but also that of AmB, for which the subcellular localization remains unknown. Based on these observations, we suggest that the sterol-rich membrane domains are also intrinsically antibiotic-sensitive, at least in fission yeast. In silico simulations, based on experimental data, have predicted that the actin cytoskeleton, exocytosis, and endocytosis all coordinate to create cell polarity (Chou et al., 2012), which in turn is most likely regulated by Cdc42 (Mogilner et al., 2012). Many protein factors involved in cell polarization have been identified. However, mutations of these genes usually affect the total cell morphogenesis. Manu-A enables quick and complete inhibition of Cdc42 activity and exocytosis, leading to the disappearance of sterol-rich antibiotic-sensitive membrane domains without the loss of cell shape polarity. This microbial metabolite could therefore prove a valuable tool for investigating the molecular mechanisms underlying the establishment and maintenance of cell morphogenesis.

EXPERIMENTAL PROCEDURES

Reagents

Filipin and AmB were purchased from Sigma-Aldrich. FM4-64 was from Invitrogen. TNM-AMCA was prepared as described previously (Ho et al., 2009). Manu-A was a gift from Kyowa Hakko Kirin. Anti-GFP antibody (GF200) was purchased from Nacalai Tesque, and anti-α-tubulin antibody (B-5-1-2) was from Sigma-Aldrich.

Yeast Strains

Deletion of the *cpp1* gene (SN246: *h⁻ leu1-32 cpp1::kan*^{r}) and *rho3* gene (SN168: *h⁻ rho3::kan*^{r}), and overexpression and tagging of Cdc42 were carried out as described in the Supplemental Experimental Procedures. An overexpression strain, *SPCC23B6.04c*, was constructed as previously reported (Matsuyama et al., 2006). Overexpression was induced in the absence of thiamine, whereas promoter activity was suppressed by the addition of thiamine (5 μM). Other strains were gifts from various yeast researchers.

Microscopy

Cells were treated with compounds at 27°C unless stated otherwise in the figure legends. Staining with filipin and TNM-AMCA were carried out as previously described (Nishimura et al., 2010; Wachtler et al., 2003). Vacuole morphology was visualized with FM4-64 as previously described (Gachet and Hyams, 2005). A MetaMorph system (Molecular Devices) was used for image acquisition together with an Olympus IX81 fluorescence microscope equipped with an UPLSAPO 100 × lens. Fluorescence intensity was quantified using the MetaMorph software.

Extraction and Analysis of Sterols

Cells were cultivated in the presence or absence of manu-A, harvested, washed with ice-cold water, and stored at −80°C until extraction. Cells (~3 × 10^7) were suspended in 75% aqueous MeOH (2 ml) containing 0.1% pyrogallol and 10 μg 4,4′-di-tert-butyl-2,2′-bipyridiyl as an internal control. $CHCl_3$ (1 ml) was added to the suspension, which was then vortexed vigorously (30 s).

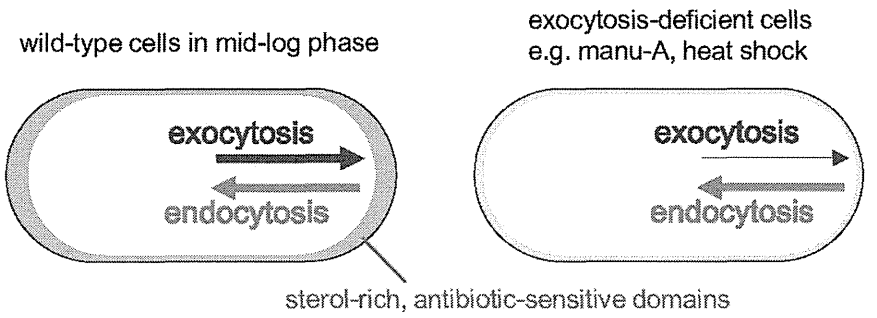

Figure 6. Model of the Production of Sterol-Rich/Antibiotic-Sensitive Plasma Membrane Domains

In actively dividing cells, exocytosis supplies sterol-rich and probably antibiotic-sensitive membrane domains to the plasma membrane. Endocytosis internalizes these domains. After the addition of manu-A or heat shock treatment, exocytosis is selectively suppressed while endocytosis is unaffected, leading to the disappearance of sterol-rich and antibiotic-sensitive membrane domains.

Petroleum ether (2 ml) was added to the mixture, followed by vortexing and centrifugation, and the upper layer was subsequently collected. This procedure was repeated twice to obtain three petroleum ether extracts. The extracts were pooled, dried over Na_2SO_4, and concentrated in vacuo. The pellet was dissolved in *N,N*-dimethylformamide (100 μl), and 2 μl of this suspension was analyzed by high performance liquid chromatography (HPLC). The HPLC conditions were as follows: column, Shiseido Capcell Pak C18 UG120 φ 4.6 × 250 at 40°C; solvent system, 85%–100% MeOH over 20 min followed by 100% MeOH for 10 min with a flow rate of 1 ml/min; and detection, 282 nm. The quantity of ergosterol detected was calculated and normalized using the internal control.

Measurement of Acid Phosphatase Secretion

Acid phosphatase secretion was assayed as described previously with some modifications (Nakano et al., 2011; Wang et al., 2002). Cells grown overnight in YE5S media at 27°C were then cultivated at 27°C overnight in Edinburgh minimal medium (EMM) media. Cells were pelleted, washed with EMM without phosphate (EMMP), and suspended in fresh EMMP. Cell cultures (at an OD_{595} of 0.2) were incubated at 27°C with or without manu-A. At each time point, 500 μl culture were centrifuged, and 400 μl of the subsequent supernatant were added to 400 μl substrate solution (2 mM *p*-nitrophenyl phosphate, 0.1 M sodium acetate, pH 4.0; prewarmed to 30°C), and the mixture was then incubated at 30°C for 5 min. Reactions were stopped by the addition of 400 μl of 1 M NaOH. The absorbance at 405 nm was measured using the medium only as a blank control, and exocytosis efficiency was calculated as the ratio of OD_{405}/OD_{595}.

Statistical Analysis

Results are shown as mean values ± SD or SE as indicated in the figure legends. Statistical significance was determined by Student's t test.

SUPPLEMENTAL INFORMATION

Supplemental Information includes Supplemental Experimental Procedures and six figures and can be found with this article online at http://dx.doi.org/10.1016/j.chembiol.2014.10.014.

ACKNOWLEDGMENTS

We thank Kyowa Hakko Kirin for the kind gift of manu-A. We are grateful to J. Ishiguro (Konan University) for the *act1/cps8* mutant strain and M. Yamamoto (The University of Tokyo) for the *pob1* mutant strain, both of which were provided through the Yeast Genetic Resource Center. We also thank R. Sugiura (Kinki University) for the *cpp1* mutant strain, H. Tatebe and K. Shiozaki (Nara Institute of Science and Technology) for the CRIB-expressing strain, M. Balasubramanian (Temasek Life Sciences Laboratory) for the lifeact-expressing strain, P. Pérez (Universidad de Salamanca) for the *cwg2* mutant strain, K.L. Gould (Vanderbilt University School of Medicine) for the *css1* mutant strain, and K. Takegawa (Kyushu University) for the ergosterol mutant strains. This work was supported in part by a Grant-in-Aid from the Japan Society for the Promotion of Science and the Ministry of Education, Culture, Sports, Science, and Technology of Japan.

Received: February 14, 2014
Revised: September 26, 2014
Accepted: October 30, 2014
Published: December 11, 2014

REFERENCES

Arenz, C., Thutewohl, M., Block, O., Waldmann, H., Altenbach, H.J., and Giannis, A. (2001). Manumycin A and its analogues are irreversible inhibitors of neutral sphingomyelinase. ChemBioChem *2*, 141–143.

Bhuiyan, M.S., Ito, Y., Nakamura, A., Tanaka, N., Fujita, K., Fukui, H., and Takegawa, K. (1999). Nystatin effects on vacuolar function in Saccharomyces cerevisiae. Biosci. Biotechnol. Biochem. *63*, 1075–1082.

Bolard, J. (1986). How do the polyene macrolide antibiotics affect the cellular membrane properties? Biochim. Biophys. Acta *864*, 257–304.

Breslow, D.K., Cameron, D.M., Collins, S.R., Schuldiner, M., Stewart-Ornstein, J., Newman, H.W., Braun, S., Madhani, H.D., Krogan, N.J., and Weissman, J.S. (2008). A comprehensive strategy enabling high-resolution functional analysis of the yeast genome. Nat. Methods *5*, 711–718.

Chou, C.S., Moore, T.I., Chang, S.D., Nie, Q., and Yi, T.M. (2012). Signaling regulated endocytosis and exocytosis lead to mating pheromone concentration dependent morphologies in yeast. FEBS Lett. *586*, 4208–4214.

Codlin, S., Haines, R.L., and Mole, S.E. (2008). btn1 affects endocytosis, polarization of sterol-rich membrane domains and polarized growth in *Schizosaccharomyces pombe*. Traffic *9*, 936–950.

Drabikowski, W., Lagwińska, E., and Sarzala, M.G. (1973). Filipin as a fluorescent probe for the location of cholesterol in the membranes of fragmented sarcoplasmic reticulum. Biochim. Biophys. Acta *291*, 61–70.

Espiritu, R.A., Matsumori, N., Murata, M., Nishimura, S., Kakeya, H., Matsunaga, S., and Yoshida, M. (2013). Interaction between the marine sponge cyclic peptide theonellamide A and sterols in lipid bilayers as viewed by surface plasmon resonance and solid state H NMR. Biochemistry *52*, 2410–2418.

Estravís, M., Rincón, S.A., Santos, B., and Pérez, P. (2011). Cdc42 regulates multiple membrane traffic events in fission yeast. Traffic *12*, 1744–1758.

Fang, Y., Hu, L., Zhou, X., Jaiseng, W., Zhang, B., Takami, T., and Kuno, T. (2012). A genomewide screen in Schizosaccharomyces pombe for genes affecting the sensitivity of antifungal drugs that target ergosterol biosynthesis. Antimicrob. Agents Chemother. *56*, 1949–1959.

Gachet, Y., and Hyams, J.S. (2005). Endocytosis in fission yeast is spatially associated with the actin cytoskeleton during polarised cell growth and cytokinesis. J. Cell Sci. *118*, 4231–4242.

Graham, T.R., Scott, P.A., and Emr, S.D. (1993). Brefeldin A reversibly blocks early but not late protein transport steps in the yeast secretory pathway. EMBO J. *12*, 869–877.

Gray, K.C., Palacios, D.S., Dailey, I., Endo, M.M., Uno, B.E., Wilcock, B.C., and Burke, M.D. (2012). Amphotericin primarily kills yeast by simply binding ergosterol. Proc. Natl. Acad. Sci. USA *109*, 2234–2239.

Hara, M., Akasaka, K., Akinaga, S., Okabe, M., Nakano, H., Gomez, R., Wood, D., Uh, M., and Tamanoi, F. (1993). Identification of Ras farnesyltransferase inhibitors by microbial screening. Proc. Natl. Acad. Sci. USA *90*, 2281–2285.

Hayles, J., and Nurse, P. (2001). A journey into space. Nat. Rev. Mol. Cell Biol. *2*, 647–656.

Ho, C.H., Magtanong, L., Barker, S.L., Gresham, D., Nishimura, S., Natarajan, P., Koh, J.L., Porter, J., Gray, C.A., Andersen, R.J., et al. (2009). A molecular barcoded yeast ORF library enables mode-of-action analysis of bioactive compounds. Nat. Biotechnol. *27*, 369–377.

Iwaki, T., Iefuji, H., Hiraga, Y., Hosomi, A., Morita, T., Giga-Hama, Y., and Takegawa, K. (2008). Multiple functions of ergosterol in the fission yeast *Schizosaccharomyces pombe*. Microbiology *154*, 830–841.

Klemm, R.W., Ejsing, C.S., Surma, M.A., Kaiser, H.J., Gerl, M.J., Sampaio, J.L., de Robillard, Q., Ferguson, C., Proszynski, T.J., Shevchenko, A., and Simons, K. (2009). Segregation of sphingolipids and sterols during formation of secretory vesicles at the trans-Golgi network. J. Cell Biol. *185*, 601–612.

Kovar, D.R., Sirotkin, V., and Lord, M. (2011). Three's company: the fission yeast actin cytoskeleton. Trends Cell Biol. *21*, 177–187.

Ma, Y., Kuno, T., Kita, A., Asayama, Y., and Sugiura, R. (2006). Rho2 is a target of the farnesyltransferase Cpp1 and acts upstream of Pmk1 mitogen-activated protein kinase signaling in fission yeast. Mol. Biol. Cell *17*, 5028–5037.

Martin, S.G., Rincón, S.A., Basu, R., Pérez, P., and Chang, F. (2007). Regulation of the formin for3p by cdc42p and bud6p. Mol. Biol. Cell *18*, 4155–4167.

Matsunaga, S., and Fusetani, N. (1995). Theonellamides A-E, cytotoxic bicyclic peptides, from a marine sponge *Theonella* sp. J. Org. Chem. *60*, 1177–1181.

Matsunaga, S., Fusetani, N., Hashimoto, K., and Walchli, M. (1989). Bioactive marine metabolites 0.26. Theonellamide F - a novel antifungal bicyclic peptide from a marine sponge *Theonella sp*. J. Am. Chem. Soc. *111*, 2582–2588.

Matsuyama, A., Arai, R., Yashiroda, Y., Shirai, A., Kamata, A., Sekido, S., Kobayashi, Y., Hashimoto, A., Hamamoto, M., Hiraoka, Y., et al. (2006). ORFeome cloning and global analysis of protein localization in the fission yeast Schizosaccharomyces pombe. Nat. Biotechnol. *24*, 841–847.

Mogilner, A., Allard, J., and Wollman, R. (2012). Cell polarity: quantitative modeling as a tool in cell biology. Science *336*, 175–179.

Muhlrad, D., and Parker, R. (1999). Aberrant mRNAs with extended 3′ UTRs are substrates for rapid degradation by mRNA surveillance. RNA *5*, 1299–1307.

Nakano, K., Toya, M., Yoneda, A., Asami, Y., Yamashita, A., Kamasawa, N., Osumi, M., and Yamamoto, M. (2011). Pob1 ensures cylindrical cell shape by coupling two distinct rho signaling events during secretory vesicle targeting. Traffic *12*, 726–739.

Nishimura, S., Arita, Y., Honda, M., Iwamoto, K., Matsuyama, A., Shirai, A., Kawasaki, H., Kakeya, H., Kobayashi, T., Matsunaga, S., and Yoshida, M. (2010). Marine antifungal theonellamides target 3β-hydroxysterol to activate Rho1 signaling. Nat. Chem. Biol. *6*, 519–526.

Nishimura, S., Ishii, K., Iwamoto, K., Arita, Y., Matsunaga, S., Ohno-Iwashita, Y., Sato, S.B., Kakeya, H., Kobayashi, T., and Yoshida, M. (2013). Visualization of sterol-rich membrane domains with fluorescently-labeled theonellamides. PLoS ONE *8*, e83716.

Park, H.O., and Bi, E. (2007). Central roles of small GTPases in the development of cell polarity in yeast and beyond. Microbiol. Mol. Biol. Rev. *71*, 48–96.

Perez, P., and Rincón, S.A. (2010). Rho GTPases: regulation of cell polarity and growth in yeasts. Biochem. J. *426*, 243–253.

Rincón, S.A., Ye, Y., Villar-Tajadura, M.A., Santos, B., Martin, S.G., and Pérez, P. (2009). Pob1 participates in the Cdc42 regulation of fission yeast actin cytoskeleton. Mol. Biol. Cell *20*, 4390–4399.

Simons, K., and Ikonen, E. (1997). Functional rafts in cell membranes. Nature *387*, 569–572.

Takeda, T., and Chang, F. (2005). Role of fission yeast myosin I in organization of sterol-rich membrane domains. Curr. Biol. *15*, 1331–1336.

Takeda, T., Kawate, T., and Chang, F. (2004). Organization of a sterol-rich membrane domain by cdc15p during cytokinesis in fission yeast. Nat. Cell Biol. *6*, 1142–1144.

Tanaka, T., Tsukuda, E., Uosaki, Y., and Matsuda, Y. (1996). EI-1511-3, -5 and EI-1625-2, novel interleukin-1 beta converting enzyme inhibitors produced by Streptomyces sp. E-1511 and E-1625. III. Biochemical properties of EI-1511-3, -5 and EI-1625-2. J. Antibiot. (Tokyo) *49*, 1085–1090.

Tatebe, H., Nakano, K., Maximo, R., and Shiozaki, K. (2008). Pom1 DYRK regulates localization of the Rga4 GAP to ensure bipolar activation of Cdc42 in fission yeast. Curr. Biol. *18*, 322–330.

Trajkovic, K., Hsu, C., Chiantia, S., Rajendran, L., Wenzel, D., Wieland, F., Schwille, P., Brügger, B., and Simons, M. (2008). Ceramide triggers budding of exosome vesicles into multivesicular endosomes. Science *319*, 1244–1247.

van Meer, G., Voelker, D.R., and Feigenson, G.W. (2008). Membrane lipids: where they are and how they behave. Nat. Rev. Mol. Cell Biol. *9*, 112–124.

Verghese, J., Abrams, J., Wang, Y., and Morano, K.A. (2012). Biology of the heat shock response and protein chaperones: budding yeast (Saccharomyces cerevisiae) as a model system. Microbiol. Mol. Biol. Rev. *76*, 115–158.

Volmer, A.A., Szpilman, A.M., and Carreira, E.M. (2010). Synthesis and biological evaluation of amphotericin B derivatives. Nat. Prod. Rep. *27*, 1329–1349.

Wachtler, V., Rajagopalan, S., and Balasubramanian, M.K. (2003). Sterol-rich plasma membrane domains in the fission yeast Schizosaccharomyces pombe. J. Cell Sci. *116*, 867–874.

Wang, H., Tang, X., Liu, J., Trautmann, S., Balasundaram, D., McCollum, D., and Balasubramanian, M.K. (2002). The multiprotein exocyst complex is essential for cell separation in *Schizosaccharomyces pombe*. Mol. Biol. Cell *13*, 515–529.

Wang, H., Tang, X., and Balasubramanian, M.K. (2003). Rho3p regulates cell separation by modulating exocyst function in *Schizosaccharomyces pombe*. Genetics *164*, 1323–1331.

Yan, Z., Costanzo, M., Heisler, L.E., Paw, J., Kaper, F., Andrews, B.J., Boone, C., Giaever, G., and Nislow, C. (2008). Yeast Barcoders: a chemogenomic application of a universal donor-strain collection carrying bar-code identifiers. Nat. Methods *5*, 719–725.

Yang, W., Urano, J., and Tamanoi, F. (2000). Protein farnesylation is critical for maintaining normal cell morphology and canavanine resistance in Schizosaccharomyces pombe. J. Biol. Chem. *275*, 429–438.

Zeeck, A., Schröder, K., Frobel, K., Grote, R., and Thiericke, R. (1987). The structure of manumycin. I. Characterization, structure elucidation and biological activity. J. Antibiot. *40*, 1530–1540.

JOC The Journal of Organic Chemistry

Article

pubs.acs.org/joc

Prediction and Determination of the Stereochemistry of the 1,3,5-Trimethyl-Substituted Alkyl Chain in Verucopeptin, a Microbial Metabolite

Aya Yoshimura, Shinji Kishimoto, Shinichi Nishimura, Saori Otsuka, Yuki Sakai, Akira Hattori, and Hideaki Kakeya*

Department of System Chemotherapy and Molecular Sciences, Division of Bioinformatics and Chemical Genomics, Graduate School of Pharmaceutical Sciences, Kyoto University, Kyoto 606-8501, Japan

Supporting Information

ABSTRACT: For the prediction of the relative stereochemistry of 1,3-dimethyl substitution in alkyl chains, a simple approach based on ^{1}H NMR data was recently proposed; $\Delta\delta$ values of methylene protons located between methyl-substituted methine carbons can be diagnostic for predicting it. Here we applied this empirical "geminal proton rule" to verucopeptin, a lipopeptide from *Streptomyces* sp. To determine the absolute stereochemistry of the 1,3,5-trimethyl-substituted alkyl chain in verucopeptin, we converted the corresponding alkyl chain to a carboxylic acid by oxidative cleavage. The geminal proton rule clearly predicted the relative stereochemistry as 31*S**,33*S**,35*R**. This prediction was definitely confirmed by synthesizing four possible diastereomers and comparing their NMR spectra. Furthermore, we reinvestigated the geminal proton rule using reported compounds and our synthesized compounds. Our result strongly suggests that the rule was solid, at least for predicting the stereochemistry of 2,4-dimethylated and 2,4,6-trimethylated fatty acids.

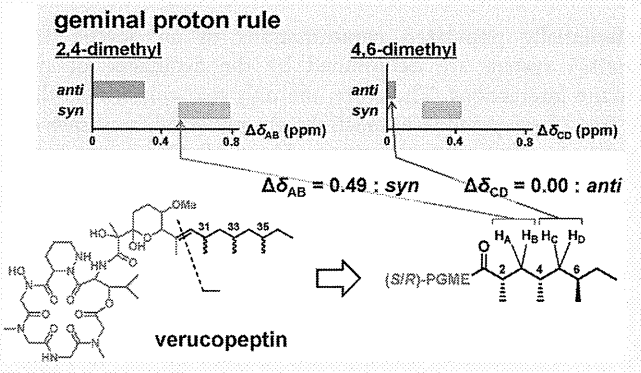

INTRODUCTION

Natural products occupy a wide chemical space and exhibit unique and sometimes medically important biological activities.[1,2] However, their complex chemical structures often hamper structure determination. For example, determination of the stereochemistry of acyclic structures is a challenging task in spite of the advancement of spectroscopic and chemical methodologies.

Several NMR techniques have been developed for determination of the stereochemistry in acyclic compounds.[3] *J*-based configurational analysis (JBCA), developed by Murata and co-workers, allows the assignment of *anti* or *gauche* relationships of two adjacent stereogenic centers.[4,5] This method exploits ^{1}H–^{1}H and ^{1}H–^{13}C coupling constants. By integrating the *J* information and NOESY correlations, we can determine relative stereochemistries of contiguous or 1,3-skipped stereogenic centers. The universal NMR database (UDB) is another powerful means constructed by Kishi and co-workers.[6−8] This database includes ^{1}H and ^{13}C NMR chemical shifts for diastereomers of polyol or related chain structures. We can compare the NMR data of a compound of interest with the database to identify the most likely diastereomer. In addition to database approaches, calculation of NMR chemical shifts is effective for predicting the stereochemistry.[3] Quantum chemistry methods can calculate NMR chemical shifts for candidate diastereomers, which can be compared with those of a molecule in question.

One of the challenging structures often found in natural products is the 1,3-dimethyl-substituted system. We can elucidate its stereochemistry by adopting JBCA, whereas measurement and/or calculation of NMR chemical shift values can predict it. However, even these excellent methods are not always applicable and alternative analytical means are required. Recently, a simple and highly sensitive method only analyzing the ^{1}H NMR data has been proposed: ^{1}H NMR chemical shifts of the methylene protons located between two methyl-bearing methine carbons in acyclic 1,3-dimethyl systems can be diagnostic (Figure 1).[9−11] In 2003, Ishibashi and co-workers noticed this phenomenon when they synthesized diastereomers of the partial structure of TT-1/rasfonin.[9] In 2010 and 2012, Breit and co-workers generalized this as an empirical rule by investigating more than 80 compounds.[10,11]

In the proposed empirical rule, when the difference of ^{1}H NMR chemical shifts for the methylene protons H_A and H_B is small, the configuration might be *anti* and vice versa (Figure 1). This rule (here we call this the "geminal proton rule") can be logically explained as described previously.[11,12] Basically, the

Received: April 24, 2014
Published: July 11, 2014

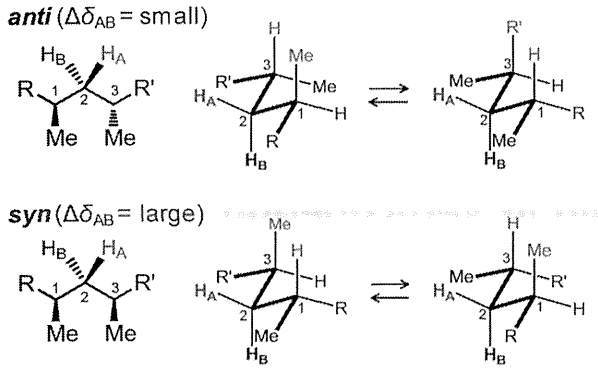

Figure 1. Conformational preference of 1,3-dimethyl-substituted structures and assignment of the relative stereochemistry. $\Delta\delta$ values for the methylene protons (H_A and H_B) are diagnostic for distinguishing the *syn* and *anti* configurations. However, the differential values are sometimes largely affected by the species of R and R′.

preferentially populated conformations of an acyclic 1,3-dimethyl system are determined by the avoidance of *syn*-pentane interactions. Therefore, the only two conformers that are free of *syn*-pentane interactions are preferred, as shown in Figure 1. In each conformer, H_A and H_B in an *anti* conformation are homotopic, each being *syn* to one proton and *syn* to one methyl group on the adjacent carbons in the chain. In contrast, the two protons in a *syn* conformation are diastereotopic, owing to a different chemical environment even when R = R′.[9] Next, R and R′ functions can affect the molecular environment experienced by H_A and H_B. This may change the absolute chemical shift values of H_A and H_B, whereas the effect against differential values between H_A and H_B in the *anti* configuration remains small, judging from the literature values for more than 80 compounds.[10,11] However, the range of differential values depends on the functional groups R and R′.[11] In addition, ambiguity can arise when compounds have bulky or shielding substituents. For a correct assignment, it is important to define the structure types that are compatible with the geminal proton rule and the corresponding differential values.

In the course of our screening for bioactive metabolites from natural sources, we isolated tumescenamide C and verucopeptin, both of which possess a 1,3-dimethyl-substituted system in acyclic structures. We reported the stereochemistry of 2,4-dimethylheptanoic acid in tumescenamide C by comparing the NMR spectra of the natural product derived compounds and synthesized authentic samples.[13] In this paper, we first confirmed the applicability of the geminal proton rule to tumescenamide C and its degradation products. We then applied the rule to verucopeptin for predicting the stereochemistry of a 1,3,5-trimethyl-substituted aliphatic chain. Analysis of the ^{1}H NMR data for the fragment structures of verucopeptin predicted the 31*S**,33*S**,35*R** stereochemistry, which was definitely confirmed by synthesizing authentic compounds. Our results indicate that the geminal proton rule is a reliable method to determine the relative stereochemistry of 2,4-dimethyl and 2,4,6-trimethyl fatty acids.

RESULTS AND DISCUSSION

2,4-Dimethyl Carboxylic Acids in Tumescenamides. Recently, we reported the isolation and structure elucidation of a cyclic lipodepsipeptide, tumescenamide C (**1**), from *Streptomyces* sp. (Figure 2a).[13] The absolute stereochemistry of

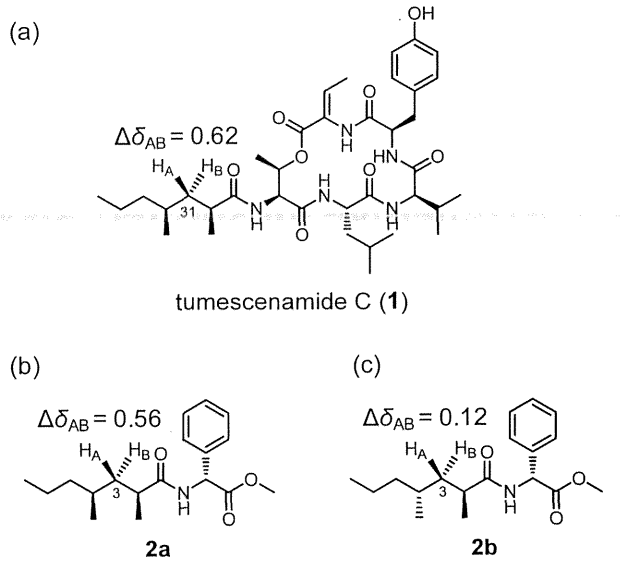

Figure 2. $\Delta\delta$ values for tumescenamide C (**1**). $\Delta\delta$ values for methylene protons at C31 for the intact natural product (a) and synthesized molecules (b, c) are shown. $\Delta\delta$ values are shown in ppm.

2,4-dimethylheptanoic acid in **1** was determined to be 2*S*,4*S* by chemical degradation and asymmetric synthesis; we synthesized the phenylglycine methyl ester (PGME) derivative **2a** and its diastereomer **2b** (Figure 2b,c) and compared their physicochemical properties with those of the PGME derivatives of 2,4-dimethylheptanoic acid that were obtained by hydrolysis of the natural product **1**. To investigate whether the geminal proton rule can be applicable to compound **1**, we reanalyzed the ^{1}H NMR chemical shift values of the methylene protons at C31. The difference of the two geminal protons was large enough (0.62 ppm), suggesting that the two methyl groups at C30 and C32 are located in a *syn* configuration (Figure 2a). This prediction was consistent with our previous results.[13] The $\Delta\delta$ values for methylene protons at C3 in synthetic **2a,b** were 0.56 and 0.12 ppm, respectively, confirming the utility of the geminal proton rule. In addition, the ^{1}H NMR spectrum of tumescenamide A, a diastereomer of tumescenamide C, also showed a large chemical shift difference (0.65 ppm) for the geminal protons at C31, suggesting the *syn* configuration of the two methyl groups.[14] This prediction was also consistent with the reported structure that was deduced by the JBCA method.[14]

NMR Analysis of Verucopeptin. Verucopeptin (**3**) is an antitumor compound originally reported from *Actinomadura verrucosospora* Q886-2.[15,16] This metabolite is composed of a cyclic depsipeptide and a polyketide side chain possessing three branched methyl groups. We reisolated verucopeptin (**3**) from the culture broth of *Streptomyces* sp. KUSC_A08. Because the stereochemistry had not been determined, we tried to predict the configuration of the 1,3,5-trimethylated alkyl chain by using the geminal proton rule. However, heavily overlapping signals due to the dynamic equilibrium between a cyclic hemiacetal form and a linear keto form hampered the complete assignment of ^{1}H NMR signals.[16] To overcome this problem, we converted compound **3** to the linear derivative **4** using $NaBH_4$ (Figure 3a).[16,17] We successfully assigned the ^{1}H NMR signals (Table S1, Supporting Information) and obtained $\Delta\delta$ values for H_2-32 and H_2-34 (Figure 3a). The $\Delta\delta$ value for H_2-34 (0 ppm) implied the *anti* relationship of the two methyl groups at C33 and C35. However, the $\Delta\delta$ value for H_2-32 (0.14 ppm) was not significant enough to predict the stereochemistry. As analyzed previously,[11] the $\Delta\delta$

dx.doi.org/10.1021/jo500906v | J. Org. Chem. 2014, 79, 6858−6867

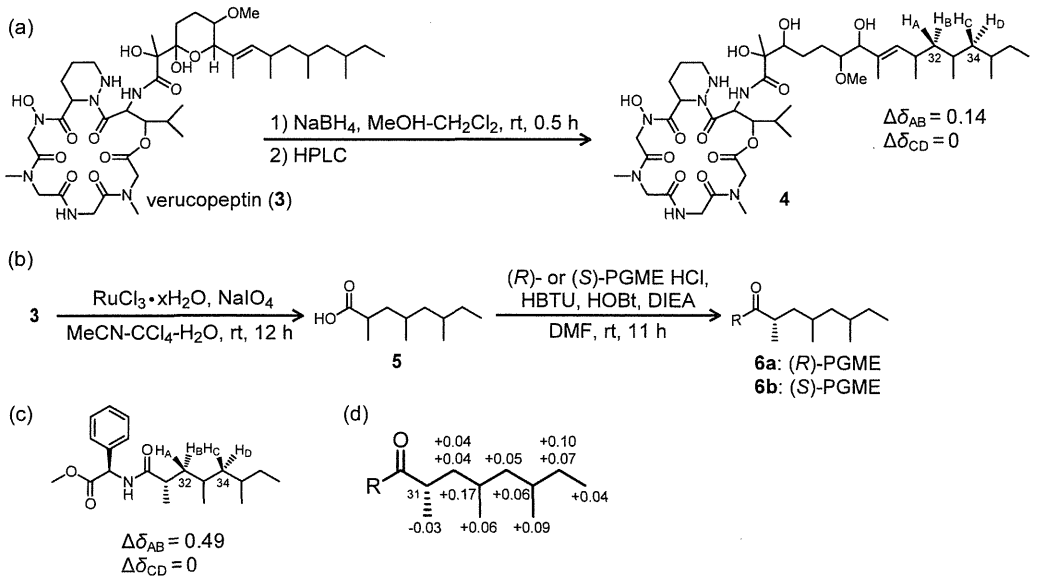

Figure 3. Prediction of the stereochemistries of C31, C33, and C35 in verucopeptin (**3**): (a) preparation of the reduced derivative **4** and $\Delta\delta$ values at C32 and C34; (b) preparation of PGME derivatives **6a,b**; (c) $\Delta\delta$ values for C32 and C34 in **6a**; (d) $\Delta\delta$ ($\delta_{(S)\text{-PGME}}$-$\delta_{(R)\text{-PGME}}$) values for **6a,b**. $\Delta\delta$ values are shown in ppm.

Scheme 1. Synthesis of (2*S*,4*S*,6*R*)-2,4,6-Trimethyloctanoic Acid (12) and Its Derivatives

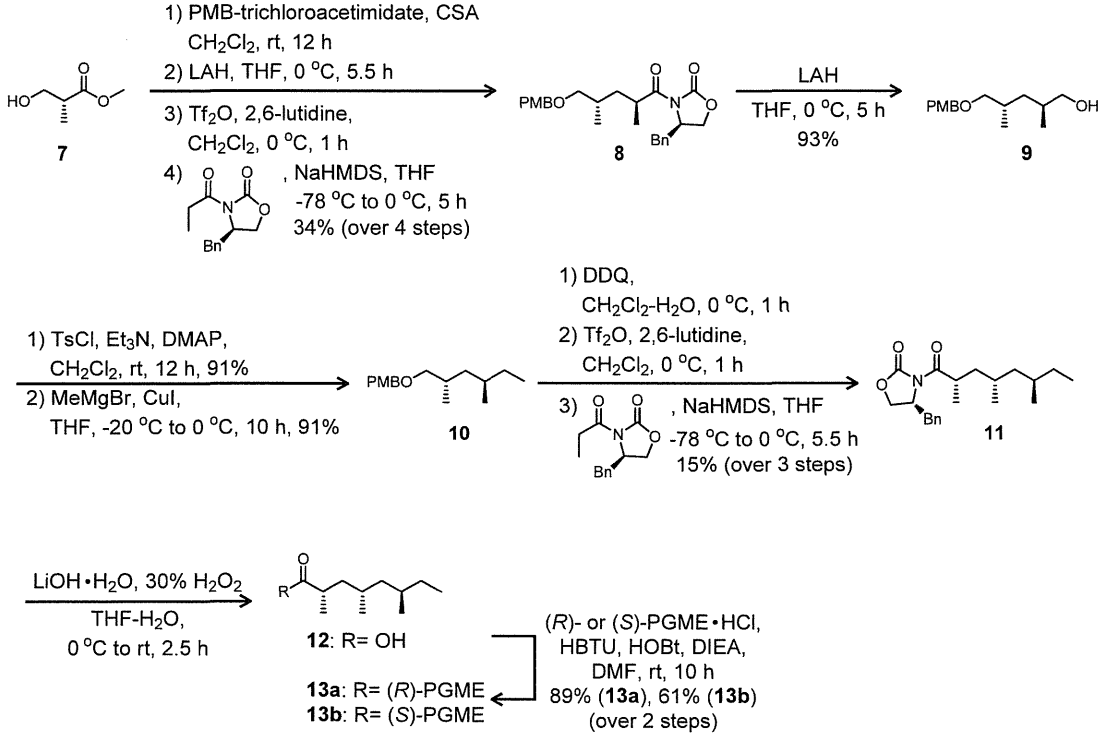

values for the *syn* configuration and those for the *anti* configuration sometimes do not show a clear difference when the alkenyl group was located just beside the methyl group. In addition, the cyclic depsipeptide portion could affect the conformation of the side chain. In fact, the $\Delta\delta$ value was very large (0.57 ppm) for the methylene protons in bitungolide A in spite of its *anti* configuration, probably because the lactone ring adjacent to the 1,3-methyl structure affects the stability of the conformer.[11] Another example is atpenin A5: a very large $\Delta\delta$ value (0.40 ppm) was observed for its *anti* configuration, which can be due to the presence of a 2,4-dihydroxy 5,6-dimethoxypyridine ring that may constrain the conformation and/or exert a magnetic shielding effect.[11]

As suggested by Breit and co-workers, and as shown above using tumescenamides, 2,4-dimethyl and 2,4,6-trimethyl carboxylic acids seem to give clear results by the geminal proton rule. Hence, we decided to obtain the side chain of compound **3** as a carboxylic acid. For this purpose, we tested several oxidation conditions: e.g., OsO_4, H_2WO_4, and $RuCl_3$. We found that oxidative cleavage using $RuCl_3$ and $NaIO_4$ successfully furnished the carboxylic acid **5**. We converted the carboxylic acid **5** to PGME derivatives **6a,b** and analyzed their

dx.doi.org/10.1021/jo500906v | J. Org. Chem. 2014, 79, 6858−6867

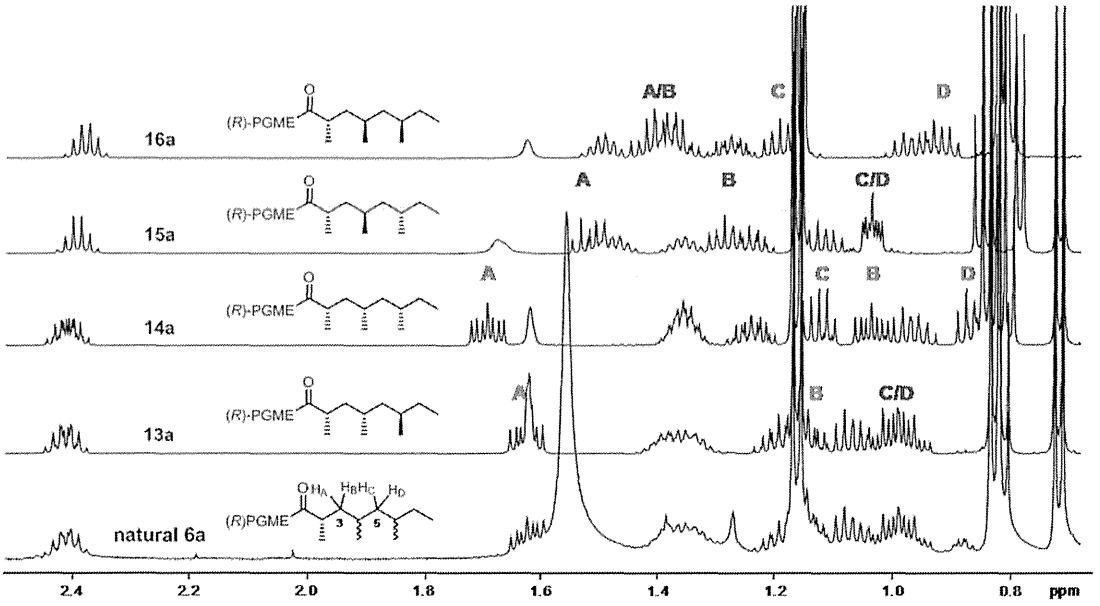

Figure 4. Comparison of the ^{1}H NMR spectra for PGME derivatives of 2,4,6-trimethyloctanoic acids. The aliphatic region of the spectra for natural product derived **6a** (natural) and the synthesized diastereomers **13a**–**16a** is shown. Red and blue indicate *anti* and *syn* configurations, respectively. Spectra were measured in $CDCl_3$ (500 MHz).

NMR spectra (Figure 3b). The $\Delta\delta$ values for positions 32 and 34 in **6a** were 0.49 and 0 ppm, respectively (Figure 3c), indicating that the three methyl groups are located in a *syn,anti* configuration. The ^{1}H NMR spectrum of **6b** gave a same result (shown in the Supporting Information).

The result obtained by the geminal proton rule was consistent with the previous prediction,[18] in which Hoffmann and co-workers calculated ^{13}C NMR chemical shift values for possible diastereomers and compared them with that of the degradation product of verucopeptin (**3**). Although the difference in the chemical shift values was subtle between *syn,anti* and *syn,syn* isomers, calculated ^{13}C NMR chemical shift values suggested that the natural product may have the former configuration. In contrast, the geminal proton rule gave more clear differences, especially in the case of fatty acid derivatives (see below). It is noted that we could determine the absolute stereochemistry of C31 by converting the carboxylic acid **5** to PGME derivatives (Figure 3d).[19] In combination with the above prediction, verucopeptin (**3**) was predicted to have an absolute stereochemistry of 31*S*,33*S*,35*R*.

Synthesis of a 2,4,6-Trimethyl Carboxylic Acid. To prove our prediction, we planned to synthesize four possible diastereomers of 2,4,6-trimethyloctanoic acid: 2*S*,4*S*,6*R*, 2*S*,4*S*,6*S*, 2*S*,4*R*,6*R*, and 2*S*,4*R*,6*S*. Our synthetic scheme for (2*S*,4*S*,6*R*)-2,4,6-trimethyloctanoic acid (**12**) is shown in Scheme 1. The synthesis of **12** was started with (*R*)-Roche ester **7**, and two stereogenic centers were constructed by stereoselective alkylation reactions using chiral oxazolidinones.[19] We first protected the hydroxyl group of Roche's ester **7** with a *p*-methoxybenzyl (PMB) group under acidic conditions, followed by reduction of the methyl ester to a hydroxyl group by LAH. The obtained alcohol was converted to a triflate, which was immediately subjected to diastereoselective alkylation by (4*R*)-propionyloxazolidinone[19] to give oxazolidinone **8** and its diastereomer.[20] Although these two diastereomers were not separated by SiO_2 column chromatography, oxazolidinone **8** was successfully purified by C18 reversed-phase HPLC (dr = 10:1). Reductive cleavage of the chiral auxiliary from oxazolidinone **8** yielded the alcohol **9**. After tosylation of the alcohol **9**, one-carbon elongation was achieved with MeMgBr and CuI to yield the protected alcohol **10**. After deprotection of PMB, a second Evans asymmetric alkylation was conducted to give oxazolidinone **11** and its diastereomer. These two diastereomers were separated by C30 reversed-phase HPLC (dr = 48:1). Purified oxazolidinone **11** was subjected to oxidative hydrolysis with alkaline hydrogen peroxide to give the carboxylic acid **12**. The carboxylic acid **12** was condensed with (*R*)- or (*S*)-PGME to give **13a,b**, respectively. Three other diastereomers and their PGME derivatives were synthesized in the same manner.

^{1}H NMR Analysis of 2,4,6-Trimethyloctanoic Acid Derivatives. With all four diastereomers in hand, we first compared ^{1}H NMR spectra of the PGME derivatives, including synthesized compounds **13a**–**16a**, and the natural product derived compound **6a** (Figure 4). The synthesized diastereomers exhibited apparently different spectra, especially signals for methylene protons at C3 and C5. The ^{1}H NMR spectrum of **6a** closely resembled that of **13a**, confirming the above prediction; we unambiguously concluded that the stereochemistry of **6a** is 31*S*,33*S*,35*R*.

We next calculated $\Delta\delta$ values for the methylene protons at C3 and C5 in the synthesized compounds **13a**–**16a** and their diastereomers **13b**–**16b** (Figure 4, compound list **S1**). The $\Delta\delta$ values of methylene protons at C3 were 0.47–0.67 ppm, when two methyl groups at C2 and C4 were located in a *syn* configuration. In contrast, the values were 0–0.23 ppm when the methyl groups were in an *anti* configuration. The difference was large enough to distinguish the relative stereochemistry of the 2,4-dimethyl carboxylic acid. The $\Delta\delta$ values of methylene protons at C5 were 0.24–0.28 ppm when in a *syn* configuration, whereas they were 0 ppm when in an *anti* configuration. Although the $\Delta\delta$ values at C5 were smaller than those at C3, the difference between *syn* and *anti* forms was apparent enough to predict the configuration.

Reinvestigation of the Geminal Proton Rule. The trends for $\Delta\delta$ values depending on functional groups adjacent to the stereogenic centers were analyzed by Breit and

dx.doi.org/10.1021/jo500906v | J. Org. Chem. 2014, 79, 6858–6867

co-workers previously.[11] We summarized the $\Delta\delta$ values of methylene geminal protons in 86 compounds, including our isolated or synthesized compounds in addition to those already analyzed by Breit and co-workers (Figure 5, bottom). The $\Delta\delta$ values for *anti* configurations were plotted between 0 and 0.4 ppm, whereas those for *syn* configurations ranged from 0.1 to 0.8 ppm, indicating that the correct stereochemistries cannot be predicted when the $\Delta\delta$ values are from 0.1 to 0.4 ppm. In contrast, such ambiguity was not observed for carboxylic acids. In the case of 1,3-dimethylated systems, the difference was apparent. We plotted 31 examples in Figure 5 (top). The $\Delta\delta$ values for CH_2-3 were larger than 0.4 ppm when 2,4-dimethyl groups were in the *syn* form. In contrast, the values were less than 0.3 ppm when the configurations were *anti*, with two exceptions: atpenin B and atenin A5. These compounds have a 2,4-dihydroxy-5,6-dimethoxypyridine ring, which seems to contribute to the unexpectedly large $\Delta\delta$ values due to the conformation constraint and/or magnetic shielding effect. We also analyzed the $\Delta\delta$ values for CH_2-5 from 17 compounds. The $\Delta\delta$ values for CH_2-5 also gave a clear result, although the values were relatively small (Figure 5, middle). The $\Delta\delta$ values were more than 0.2 when 4,6-dimethyl groups were in *syn* configurations. The values were almost 0 when the configurations were *anti*. These data revealed that the geminal proton rule is reliable in 2,4-dimethyl and 2,4,6-trimethyl fatty acids. By using this rule, we could predict the relative stereochemistry of the acyl group in another tumescenamide congener, tumescenamide B (**17**),[8] whose configuration has not been determined (Figure 6). The $\Delta\delta$ values for CH_2-31 and -33 were 0.75 and 0.34, respectively, suggesting the *syn,syn* configuration.

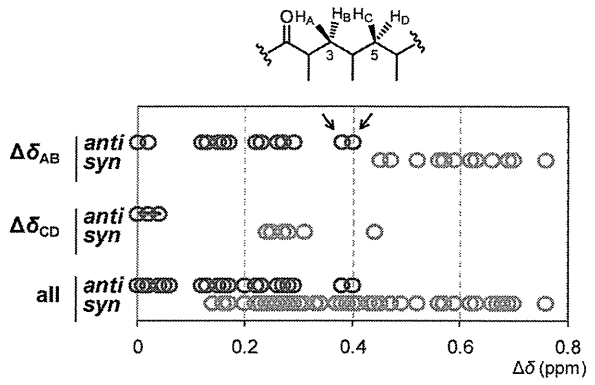

Figure 5. Tendencies for $\Delta\delta$ values. Values for *syn* configurations are plotted in blue and *anti* in red. $\Delta\delta$ values for H_A and H_B (31 compounds, top), $\Delta\delta$ value for H_C and H_D (17 compounds, middle), and $\Delta\delta$ values for any methylene protons located between methyl-bearing methane carbons (86 compunds, bottom) are plotted. Arrows indicate exceptionally large values for atpenin B and atpenin A5, as mentioned in the text. The compound list is included in the Supporting Information.

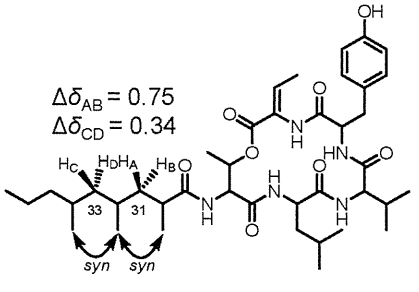

Figure 6. Structure of tumescenamide B (**17**) with proposed stereochemistry. The $\Delta\delta$ values for C31 and C33 are shown in ppm.

CONCLUSION

We have reinvestigated the utility of an empirical NMR approach, the geminal proton rule, for determination of the configuration of 1,3-dimethylated systems. Our data indicated that the emerging rule is highly reliable when predicting the stereochemistry of 2,4-dimethyl or 2,4,6-trimethyl fatty acids. In fact, the stereochemistry of the 1,3,5-trimethylated system in verucopeptin (**3**) was successfully predicted after conversion of the system to a 2,4,6-trimethyl fatty acids. In addition, we could deduce the relative stereochemistry of the acyl chain in tumescenamide B (**17**) from the reported NMR data. So far, many natural products with methyl branched fatty acids have been reported. There remain many compounds with unknown stereochemistries: e.g., dactylfungins[21] and totopotensamides.[22] The geminal proton rule would be helpful for elucidating the stereochemistry of such compounds.

EXPERIMENTAL SECTION

General Considerations. All reagents and solvents were used as received from commercial suppliers and were used without further purification. IR spectra were measured using an FTIR spectrometer equipped with a ZnSe ATR plate. Optical rotations were determined using the sodium D line (589 nm). NMR spectra were measured on a 500 MHz instrument. ^1H and ^{13}C chemical shifts are shown relative to the solvent: δ_H 7.26 and δ_C 77.0 for $CDCl_3$. Chemical shifts (δ) are shown in parts per million (ppm), and coupling constants (J) are in hertz (Hz). The following abbreviations are used to describe multiplicities: s, singlet; d, doublet; dd, doublet of doublets; m, multiplet. Mass spectral data were collected with FAB MS or ESI IT-TOF MS. Flash column chromatography was performed over Silica Flash F60 (SiliCycle) using an elution system as described for each experiment.

Isolation of Verucopeptin (3). *n*-BuOH extracts of the culture broth of *Streptomyces* sp. KUSC_A08 (16 L) were extracted with 90% MeOH three times. The combined extracts were evaporated and extracted with $CHCl_3$ three times. The $CHCl_3$ extracts were combined and concentrated in vacuo. The residue was dissolved in $CHCl_3$/MeOH (50/50) and fractionated on a LH-20 gel filtration column with $CHCl_3$/MeOH (50/50). Fractions containing verucopeptin were combined and chromatographed on a silica gel column with $CHCl_3$/MeOH (45/1 to 20/1). Fractions eluted by $CHCl_3$/MeOH (45/1) were subjected to ODS HPLC on CAPCELL PAK UG120 (i.d. 20 × 250 mm) with MeCN/H_2O (75/25) to afford verucopeptin (**3**; 121.61 mg) as a colorless amorphous solid: $[\alpha]_D^{20}$ = = −91.0° (*c* 0.12, $CHCl_3$); IR (neat) 3352, 2955, 1644, 1406, 1241, 754 cm^{-1}; ^1H NMR for the major acetal form ($CDCl_3$, 500 MHz) δ 9.11 (*N*-OH), 7.32 (d, J = 9.7 Hz), 7.12 (d, J = 5.9 Hz), 6.08 (dd, J = 9.8, 3.1 Hz, 1H), 5.31 (m, 1H), 5.27 (d, J = 15.5 Hz, 1H), 5.16 (m, 1H), 5.04 (d, J = 16.9 Hz, 1H), 4.90 (m, 1H), 4.77 (dd, J = 9.8, 3.1 Hz, 1H), 4.64 (d, J = 16.3 Hz, 1H), 4.11 (m, 1H), 4.09 (m), 3.88 (d, J = 15.5 Hz, 1H), 3.65 (dd, J = 17.2, 6.5 Hz, 1H), 3.55 (d, J = 17.2 Hz, 1H), 3.44 (m), 3.28 (s, 3H), 3.11 (s, 3H/m), 3.04 (m, 1H), 2.91 (s, 3H), 2.65 (m, 1H), 2.51 (m, 1H), 2.17 (m, 1H), 2.03 (m, 1H), 1.87 (m), 1.80 (m), 1.72 (m), 1.65 (s), 1.57 (m), 1.50 (m), 1.46 (m), 1.40 (s, 3H),1.37 (m), 1.26 (m), 1.20 (m), 1.13 (m), 1.06 (d, J = 6.7 Hz), 1.02 (m), 0.97 (d, J = 6.7 Hz), 0.86 (m), 0.84 (m), 0.80 (m), 0.77 (m); ^{13}C NMR for the major acetal form ($CDCl_3$, 125 MHz) δ 176.2, 172.0, 171.3, 170.8, 170.2, 167.1, 166.8, 137.0, 130.0, 98.4, 80.0, 79.6, 77.6, 75.7, 56.8, 52.5, 51.7, 51.3, 48.4, 46.9, 46.5, 46.1, 45.0, 42.4, 36.7, 34.7, 31.7, 30.4 (2C), 29.6, 27.7, 27.2, 24.1, 23.9, 21.3 (2C), 20.5, 19.4, 19.2, 19.1, 18.3, 11.4; HRMS (ESI) m/z 918.5169 $[M + Na]^+$ calcd for $C_{43}H_{73}N_7NaO_{13}$, 918.5159. ^1H and ^{13}C NMR chemical shifts were in agreement with those reported previously.[23]

dx.doi.org/10.1021/jo500906v | J. Org. Chem. 2014, 79, 6858−6867

Reduction of 3. To a stirred solution of verucopeptin (3; 8.88 mg, 9.92×10^{-3} mmol) in $CHCl_3$/MeOH (1/1, 1.98 mL) was added $NaBH_4$ (5.62 mg, 0.15 mmol) at room temperature. After 30 min, PBS buffer was added to the reaction mixture. The organic layer was washed with PBS buffer (three times) and concentrated in vacuo. The residue was chromatographed on an ODS column with a stepwise elution of H_2O/MeOH (from 100/0 to 0/100). Fractions eluted with H_2O/MeOH (10/90 and 0/100) were combined and subjected to ODS HPLC on Cosmosil AR-II-C18 (i.d. 20 × 250 mm) with H_2O/MeCN (40/60) to afford the reduced verucopeptin derivative **4** (4.92 mg, 55%) as a colorless amorphous solid: $[\alpha]_D^{20} = -151.7°$ (*c* 0.06, $CHCl_3$); IR (neat) 3344, 2958, 2926, 1648 cm^{-1}; ^1H NMR ($CDCl_3$, 500 MHz) δ 7.08 (NH), 7.04 (NH), 6.12 (dd, *J* = 3.0, 8.9 Hz, 1H), 5.27 (d, *J* = 15.2 Hz, 1H), 5.24 (m, 1H), 5.23 (m, 1H), 4.98 (dd, *J* = 2.9, 10.0 Hz, 1H), 4.92 (m, 1H), 4.78 (NH), 4.71 (d, *J* = 17.3 Hz, 1H), 4.15 (m, 1H), 4.13 (m, 1H), 3.88 (d, *J* = 15.5 Hz, 1H), 3.65 (dd, *J* = 4.1, 17.5 Hz, 2H), 3.44 (m, 1H), 3.43 (m, 1H), 3.40 (s, 3H), 3.28 (m, 1H), 3.11 (s, 3H/m, 1H), 2.91 (s, 3H), 2.67 (m, 1H), 2.51 (m, 1H), 2.23 (m, 1H), 1.87 (m, 1H), 1.79 (m, 1H), 1.76 (m, 1H), 1.70 (m, 2H), 1.63 (s, 3H) 1.60 (m, 1H), 1.56 (m, 1H), 1.46 (m, 1H), 1.41 (s, 3H), 1.39 (m, 1H), 1.25 (m, 1H), 1.20 (m, 1H), 1.15 (m, 1H), 1.11 (d, *J* = 6.8 Hz, 3H), 1.06 (m, 1H), 1.02 (m, 2H), 0.91 (d, *J* = 6.5 Hz, 3H), 0.88 (s, 3H), 0.85 (m, 3H), 0.80 (m, 3H), 0.79 (m, 3H); ^{13}C NMR ($CDCl_3$, 125 MHz) δ 174.8, 171.6 171.4, 170.8, 170.7, 168.5, 167.0, 134,1 131.7, 82.3, 80.2, 76.7, 76.1, 57.6, 52.7, 51.7, 51.4, 48.8, 47.2, 46.9, 46.0, 44.8, 42.3, 36.6, 34.7, 31.7, 30.4, 29.7, 29.5, 27.9, 26.9, 26.0, 23.9, 21.4 (2C), 20.1, 19.5, 19.3, 19.0, 18.5, 13.1, 11.4; HRMS (ESI) *m*/*z* 920.5334 $[M + Na]^+$ calcd for $C_{43}H_{75}N_7NaO_{13}$, 920.5315.

PGME Derivatives of the Natural Trimethyloctanoic Acid (6a,b). To a stirred solution of **3** (4.26 mg, 4.76×10^{-3} mmol) in MeCN/CCl_4/H_2O (2/2/3, 0.32 mL) were added $RuCl_3 \cdot xH_2O$ (6.50 mg, 0.03 mmol) and $NaIO_4$ (41.46 mg, 0.19 mmol). After the mixture was stirred at room temperature for 12 h, water was added. The mixture was chromatographed on an ODS column with a stepwise elution of H_2O/MeOH (from 100/0 to 0/100). Fractions eluted with H_2O/MeOH (40/60 to 0/100) were combined and concentrated in vacuo. The material was split into two portions. One portion of the material was mixed with HBTU (13.73 mg, 0.04 mmol), HOBt (6.17 mg, 0.05 mmol), DIEA (11.0 μL, 0.06 mmol), and (*R*)-PGME·HCl (7.86 mg, 0.04 mmol) in DMF (0.11 mL), which was stirred at room temperature. After 9 h, saturated aqueous NH_4Cl was added to the reaction mixture. The organic layer was washed with saturated aqueous NH_4Cl (three times) and concentrated in vacuo. The obtained residue was chromatographed on an ODS column with a stepwise elution of H_2O/MeOH (from 100/0 to 0/100) and $CHCl_3$/MeOH (1/1). Fractions eluted with H_2O/MeOH (0/100) were subjected to ODS HPLC on CAPCELL PACK C18 UG120 (i.d. 20 × 250 mm) with H_2O/MeCN (50/50) to afford **6a** (0.25 mg, 32%).

The remaining portion of the carboxylic acid (0.88 mg) was mixed with HBTU (19.63 mg, 0.05 mmol), HOBt (8.06 mg, 0.06 mmol), DIEA (16.35 μL, 0.1 mmol), and (*S*)-PGME·HCl (11.72 mg, 0.06 mmol) in DMF (0.16 mL), which was stirred for 11 h at room temperature. The reaction mixture was fractionated as described above to afford **6b** (0.25 mg, 32%).

*Compound **6a**:* $[\alpha]_D^{20} = -84.64°$ (*c* 0.02, $CHCl_3$); IR (neat) 3314, 2957, 2922, 2849, 1746, 1648, 1523 cm^{-1}; ^1H NMR ($CDCl_3$, 500 MHz) δ 7.29–7.37 (5H), 6.4 (NH), 5.60 (d, *J* = 7.2 Hz, 1H), 3.73 (s, 3H), 2.39 (m, 1H), 1.61 (m, 1H), 1.37 (m, 1H), 1.33 (m, 1H), 1.16 (m, 1H), 1.14 (d, *J* = 6.9 Hz, 3H), 1.13 (m, 1H), 0.98 (m, 2H), 0.81 (d, *J* = 6.9 Hz, 3H/t, *J* = 6.9 Hz, 3H), 0.70 (d, *J* = 6.6 Hz, 3H); ^{13}C NMR ($CDCl_3$, 125 MHz) δ 176.2, 171.9, 128.9, 128.4, 127.2, 56.1, 52.8, 44.3, 42.6, 38.8, 31.5, 30.2, 27.8, 19.4, 18.8, 18.3, 11.3; HRMS (ESI) *m*/*z* 356.2196 $[M + Na]^+$ calcd for $C_{20}H_{31}NNaO_3$, 356.2196.

*Compound **6b**:* $[\alpha]_D^{20} = 154.73°$ (*c* 0.02, $CHCl_3$); IR (neat) 3293, 2960, 2927, 1748, 1647, 1527 cm^{-1}; ^1H NMR ($CDCl_3$, 500 MHz) δ 7.30–7.37 (5H), 6.36 (NH), 5.59 (d, J= 7.3 Hz, 1H), 3.73 (s, 3H), 2.41 (m, 1H), 1.64 (m, 1H), 1.54 (m, 1H), 1.39 (m, 1H), 1.26 (m, 1H), 1.17 (m, 1H), 1.14 (m, 1H), 1.11 (d, *J* = 7.1 Hz, 3H), 1.03 (m, 2H), 0.87 (d, *J* = 6.3 Hz, 3H), 0.85 (t, *J* = 7.4 Hz, 3H), 0.79 (d, *J* = 6.4 Hz, 3H); ^{13}C NMR ($CDCl_3$, 125 MHz) δ 175.9, 171.5, 129.0, 128.5, 127.2, 56.1, 52.7, 44.3, 42.5, 38.8, 31.6, 30.4, 27.9, 19.6, 18.9, 18.3, 11.4; HRMS (ESI) *m*/*z* 356.2191 $[M + Na]^+$ calcd for $C_{20}H_{31}NNaO_3$, 356.2196.

PGME Derivatives of Synthetic (2*S*,4*S*,6*R*)-Trimethyloctanoic Acid (13a,b). *(R)-4-Benzyl-3-((2S,4S)-5-((4-methoxybenzyl)oxy)-2,4-dimethylpentanoyl)oxazolidin-2-one (**8**).* To a stirred solution of methyl (*S*)-3-hydroxyisobutyrate (2.0 g, 16.90 mmol) in anhydrous CH_2Cl_2 (33.90 mL) were added CSA (0.33 g, 1.42 mmol) and PMB trichloroacetimidate (5.27 mL, 25.40 mmol). After the mixture was stirred for 12 h at room temperature, the reaction was quenched by addition of saturated aqueous $NaHCO_3$. The mixture was extracted with $CHCl_3$, washed with brine, dried over Na_2SO_4, and concentrated in vacuo. The residue in cooled hexane was filtered through Celite and concentrated in vacuo. The residue was suspended in *n*-hexane/EtOAc (10/1), filtered through a pad of silica, and used in the next reaction.

A solution of the residue (4.0 g) in anhydrous THF (84.50 mL) was cooled to 0 °C under a nitrogen atmosphere, to which LAH (0.67 g, 17.60 mmol) was added. After the reaction mixture was stirred for 5.5 h at 0 °C, it was quenched with $Na_2SO_4 \cdot 10H_2O$ and the slurry was stirred at room temperature. The mixture was filtered through a pad of silica and washed with $CHCl_3$. After concentration in vacuo, the residue was chromatographed (SiO_2, *n*-hexane/EtOAc 5/1 to 1/1) to give fractions that contained the target alcohol.

A stirred solution of the obtained alcohol (0.11 g) in 1.10 mL of anhydrous CH_2Cl_2 under a nitrogen atmosphere was cooled to 0 °C, and 2,6-lutidine (0.11 mL, 0.81 mmol) and Tf_2O (0.14 mL, 0.81 mmol) were added. After the mixture was stirred for 1 h at 0 °C, the reaction was quenched with saturated aqueous NH_4Cl. The organic layer was washed with saturated aqueous NH_4Cl, saturated aqueous $NaHCO_3$ and brine, dried over anhydrous Na_2SO_4, and concentrated in vacuo. The residue was chromatographed (SiO_2, *n*-hexane/EtOAc 10/1) to give fractions containing the triflate compound. The fractions were combined and concentrated, and the residue was immediately used in the next reaction.

A stirred solution of (*R*)-4-benzyl-3-propionyl-2-oxazolidinone (99.80 mg, 0.54 mmol) in anhydrous THF (5.40 mL) under a nitrogen atmosphere was cooled to −78 °C, and 0.34 mL of 1.9 M NaHMDS was added. After the mixture was stirred for 15 min at −78 °C, the triflate compound (0.22 g) in 21.60 mL of anhydrous THF was added dropwise. The reaction mixture was stirred at −78 °C, warmed to 0 °C, stirred for 5 h, and then quenched with saturated aqueous NH_4Cl. The aqueous layer was extracted with $CHCl_3$, and the combined organic layers were dried over anhydrous Na_2SO_4 and concentrated in vacuo. The residue was chromatographed (SiO_2, *n*-hexane/EtOAc 5/1) to give a mixture of **8** and its diastereomer. The mixture was subjected to reversed-phase HPLC (Cosmosil AR-II, i.d. 20 × 250 mm, H_2O/MeCN (35/65)) to give **8** (74.90 mg, 40%) as a colorless oil. The ratio of **8** and its diastereomer was 11:1, as judged from their yield. Compound **8**: $[\alpha]_D^{20} = -5.97°$ (*c* 1.10, $CHCl_3$); IR (neat) 2932, 2856, 1776, 1206, 701 cm^{-1}; ^1H NMR ($CDCl_3$, 500 MHz) δ 6.86–7.34 (m, 9H), 4.64 (m, 1H), 4.42 (d, *J* = 4.6 Hz, 2H), 4.15 (dd, *J* = 8.5 Hz, 1H), 4.08 (dd, *J* = 3.3, 9.1 Hz, 1H), 3.88 (m, 1H), 3.80 (s, 3H), 3.29 (m, 2H), 3.26 (m, 1H), 2.50 (dd, *J* = 10.5, 13.4 Hz, 1H), 1.88 (m, 1H), 1.66 (ddd, *J* = 7.2, 8.2, 14.0 Hz, 1H), 1.51 (ddd, *J* = 6.6, 8.7, 14.0 Hz, 1H), 1.16 (d, *J* = 6.4 Hz, 3H), 0.96 (d, *J* = 7.2 Hz, 3H); ^{13}C NMR ($CDCl_3$, 125 MHz) δ 177.4, 159.0, 153.0, 135.5, 130.7, 129.34, 129.31, 128.8, 127.2, 113.7, 75.8, 72.7, 65.89, 55.3, 55.2, 38.0, 37.8, 35.3, 31.3, 17.06 (2C); HRMS (ESI) *m*/*z* 448.2111 $[M + Na]^+$ calcd for $C_{25}H_{31}NNaO_5$, 448.2094.

*(2S,4S)-5-((4-Methoxybenzyl)oxy)-2,4-dimethylpentan-1-ol (**9**).* A stirred solution of **8** (0.17 g, 0.39 mmol) in anhydrous THF (1.90 mL) under a nitrogen atmosphere was cooled to 0 °C, and LAH (18.0 mg, 0.48 mmol) was added. After the mixture was stirred for 5 h at 0 °C, the reaction was quenched with $Na_2SO_4 \cdot 10H_2O$ and the slurry was stirred at room temperature. The mixture was filtered through a pad of silica and washed with EtOAc. After concentration in vacuo, the residue was chromatographed (SiO_2, *n*-hexane/EtOAc 3/1 to 2/1) to yield **9** (90.77 mg, 93%) as a colorless oil: $[\alpha]_D^{20} = -14.4°$ (*c* 0.98, $CHCl_3$); IR (neat) 3410, 2910, 2851, 1244, 1033, 818 cm^{-1}; ^1H NMR ($CDCl_3$, 500 MHz) δ 7.24 (d, *J* = 8.8 Hz, 2H), 6.87 (d, *J* = 8.6 Hz,

dx.doi.org/10.1021/jo500906v | J. Org. Chem. 2014, 79, 6858–6867

2H), 4.42 (s, 2H), 3.79 (s, 3H), 3.44 (dd, J = 6.4, 10.5 Hz, 1H), 3.39 (dd, J = 6.4, 10.7 Hz, 1H), 3.26 (dd, J = 6.7, 9.0 Hz, 1H), 3.23 (dd, J = 6.3, 9.0 Hz, 1H), 1.87 (m, 1H), 1.73 (m, 1H), 1.19 (m, 2H), 0.89 (d, J = 7.1 Hz, 3H), 0.88 (d, J = 7.3 Hz, 3H); ^{13}C NMR ($CDCl_3$, 125 MHz) δ 159.0, 130.6, 129.1, 113.7, 76.2, 72.6, 68.7, 55.2, 37.2, 32.9, 30.5, 16.9, 16.3; HRMS (ESI) m/z 275.1619 $[M + Na]^+$ calcd for $C_{15}H_{24}NaO_3$, 275.1618.

*1-((((2S,4R)-2,4-Dimethylhexyl)oxy)methyl)-4-methoxybenzene (**10**).* To a stirred solution of **9** (0.65 g, 2.59 mmol) in 17.30 mL of anhydrous CH_2Cl_2 under a nitrogen atmosphere were added Et_3N (0.90 mL, 6.48 mmol), DMAP (32.0 mg, 0.26 mmol), and TsCl (0.60 g, 3.17 mmol) at room temperature. After the mixture was stirred for 12 h, saturated aqueous NH_4Cl was added. The organic layer was dried over anhydrous Na_2SO_4 and concentrated in vacuo. The residue was chromatographed (SiO_2, n-hexane/EtOAc 5/1) to give fractions containing tosylated compounds.

A mixture of CuI (0.45 g, 2.34 mmol) and 1 M MeMgBr (23.40 mL, 23.40 mmol) was cooled to −20 °C under a nitrogen atmosphere, and the tosylated material (0.95 g) in anhydrous THF was added. The mixture was warmed to 0 °C and stirred for 10 h. The reaction was quenched with saturated aqueous NH_4Cl and filtered through Celite. The organic layer was washed with saturated aqueous NH_4Cl, dried over anhydrous Na_2SO_4, and concentrated in vacuo. The residue was chromatopraphed (SiO_2, n-hexane/EtOAc 50/1) to yield **10** (0.53 g, 83% over two steps) as a colorless oil: $[\alpha]_D^{20}$ = −11.75° (c 1.03, $CHCl_3$); IR (neat) 2957, 2911, 1512, 1245, 1096, 819 cm^{-1}; ^{1}H NMR ($CDCl_3$, 500 MHz) δ 7.31 (d, J = 9.0 Hz, 2H), 6.92 (d, J = 8.7 Hz, 2H), 4.48 (d, J = 2.6 Hz, 2H), 3.81 (s, 3H), 3.34 (dd, J = 5.7, 8.9 Hz, 1H), 325 (dd, J = 7.4, 9.2 Hz, 1H), 1.91 (m, 1H), 1.48 (m, 1H), 1.37 (m, 1H), 1.23 (m, 1H), 1.22 (m, 1H), 1.15 (m, 1H), 0.97 (d, J = 6.8 z, 3H), 0.93 (t, J = 7.4 Hz, 3H), 0.90 (d, J = 6.6 Hz, 3H); ^{13}C NMR ($CDCl_3$, 125 MHz) δ 158.9, 130.8, 128,8, 113.5, 76.3, 72.5, 54.9, 40.6, 31.5, 30.8, 30.3, 18.8, 16.9, 11.3; HRMS (ESI) m/z 273.1821 $[M + Na]^+$ calcd for $C_{16}H_{26}NaO_2$, 273.1825.

*(R)-4-Benzyl-3-((2S,4S,6R)-2,4,6-trimethyloctanoyl)oxazolidin-2-one (**11**).* A stirred solution of **10** (0.24 g, 0.95 mmol) in CH_2Cl_2/H_2O (15/1, 9.50 mL) was cooled to 0 °C, and DDQ (0.33 g, 1.44 mmol) was added. After the mixture was stirred for 1 h at 0 °C, the reaction was quenched with saturated aqueous $NaHCO_3$. The organic layer was washed with saturated aqueous $NaHCO_3$, dried over anhydrous Na_2SO_4, and concentrated in vacuo. The residue was chromatographed (SiO_2, n-hexane/Et_2O 4/1) to give a fraction that contained the target alcohol.

A stirred solution of the obtained material (0.28 g) in anhydrous CH_2Cl_2 (4.40 mL) under a nitrogen atmosphere was cooled to 0 °C, and 2,6-lutidine (0.45 g, 3.27 mmol) and Tf_2O (0.55 g, 3.27 mmol) were added. After the mixture was stirred for 1 h at 0 °C, the reaction was quenched with saturated aqueous NH_4Cl. The organic layer was washed with saturated aqueous NH_4Cl, saturated aqueous $NaHCO_3$, and brine, dried over anhydrous Na_2SO_4, and concentrated in vacuo. The residue was chromatographed (SiO_2, n-hexane/EtOAc 20/1) to give a fraction that contained triflated material. The fraction was concentrated in vacuo, and the residue was immediately used in the next reaction.

A stirred solution of (*R*)-4-benzyl-3-propionyl-2-oxazolidinone (0.16 g, 0.71 mmol) in anhydrous THF (7.10 mL) under a nitrogen atmosphere was cooled to −78 °C, and 0.45 mL of 1.9 M NaHMDS was added. After the mixture was stirred for 15 min at −78 °C, the triflated material (0.12 g) in 15.10 mL of anhydrous THF was added dropwise. The reaction mixture was stirred at −78 °C, warmed to 0 °C, stirred for 5.5 h, and then quenched with saturated aqueous NH_4Cl. The aqueous layer was extracted with $CHCl_3$, and the combined organic layers were dried over anhydrous Na_2SO_4 and concentrated in vacuo. The residue was chromatographed (SiO_2, n-hexane/EtOAc 5/1) to give a mixture of **11** and its diastereomer. The mixture was subjected to reversed-phase HPLC (YMC Carotenoid, i.d. 20 × 250 mm, H_2O/MeCN (35/65)) to yield **11** (50.6 mg, 15% over three steps) as a colorless oil. The ratio of **11** and its diastereomer was 48:1, as judged from their yield: $[\alpha]_D^{20}$ = −37.88° (c 2.32, $CHCl_3$); IR (neat) 2959, 2924, 1779, 1697, 1384, 1206, 701 cm^{-1}; ^{1}H NMR ($CDCl_3$, 500 MHz) δ 7.19–7.35 (5H), 4.68 (m, 1H), 4.17 (m, 2H), 3.94 (m, 1H), 3.29 (dd, J = 3.6, 13.5 Hz, 1H), 2.72 (dd, J = 9.7, 13.3 Hz, 1H), 1.82 (ddd, J = b 6.4, 8.1, 14.1 Hz, 1H), 1.55 (m, 1H), 1.42 (m, 1H), 1.27 (m, 1H), 1.22 (m, 1H), 1.16 (m, 1H/d, J = 6.7 Hz, 3H), 1.16 (d, J = 6.7 Hz, 3H), 1.10 (m, 2H), 0.89 (d, J = 6.8 Hz, 3H), 0.86 (t, J = 7.5 Hz, 3H), 0.82 (d, J = 12.4 Hz, 3H); ^{13}C NMR ($CDCl_3$, 125 MHz) δ 177.7, 153.0, 135.4, 129.4, 128.9, 127.3, 65.9, 55.3, 43.9, 42.1, 38.0, 35.2, 31.6, 30.3, 28.2, 19.8, 18.9, 17.8, 11.4; HRMS (ESI) m/z 368.2197 $[M + Na]^+$ calcd for $C_{21}H_{31}NNaO_3$, 368.2196.

*(R)-Methyl-2-phenyl-2-((2S,4S,6R)-2,4,6-trimethyloctamido)-acetate (**13a**).* To a stirred solution of **11** (24.90 mg, 5.85 × 10^{-2} mmol) in THF/H_2O (4/1, 0.98 mL) was added LiOH·H_2O (7.36 mg, 0.18 mmol) and 30% aqueous H_2O_2 (66.30 μL, 0.59 mmol) at 0 °C. The mixture was stirred for 1 h at 0 °C, warmed to room temperature, stirred for 2.5 h, and then quenched with saturated aqueous $Na_2S_2O_3$. After being acidified with 6 N HCl, the reaction mixture was extracted with $CHCl_3$. The organic layers were combined and concentrated in vacuo to give a residue containing **12**.

A half-portion of the material above containing **12** (18.20 mg), HBTU (76.80 mg, 0.20 mmol), HOBt (31.10 mg, 0.20 mmol), DIEA (33.70 mL, 0.20 mmol), and (*R*)-PGME·HCl (42.60 mg, 0.21 mmol) were dissolved in 0.98 mL of anhydrous DMF, and this mixture was stirred for 10 h at room temperature. The reaction was quenched with saturated aqueous NH_4Cl, dried over anhydrous Na_2SO_4, and concentrated in vacuo. The residue was chromatographed (SiO_2, n-hexane/EtOAc 3/1) to yield **13a** (8.70 mg, 89%) as a colorless amorphous solid: $[\alpha]_D^{20}$ = −127.05° (c 0.72, $CHCl_3$); IR (neat) 2959, 2924, 1779, 1697, 1384, 1206, 701 cm^{-1}; ^{1}H NMR ($CDCl_3$, 500 MHz) δ 7.29–7.36 (5H), 6.42 (NH), 5.60 (d, J = 7.5 Hz, 1H), 3.73 (s, 3H), 2.39 (m, 1H), 1.61 (m, 1H), 1.37 (m, 1H), 1.32 (m, 1H), 1.16 (m, 1H), 1.15 (d, J = 7.0 Hz, 3H), 1.12 (m, 1H), 1.07 (m, 1H), 0.97 (m, 2H), 0.81 (d, J = 7.4 Hz, 3H), 0.80 (t, J = 7.4 Hz, 3H), 0.70 (d, J = 7.0 Hz, 3H); ^{13}C NMR ($CDCl_3$, 125 MHz) δ 175.9, 171.5, 136.8, 128.9, 128.4, 127.2, 56.1, 52.7, 44.3, 42.7, 38.8, 31.5, 30.2, 27.9, 19.4, 18.8, 18.3, 11.3; HRMS (ESI) m/z 356.2200 $[M + Na]^+$ calcd for $C_{20}H_{31}NNaO_3$, 356.2196.

*(S)-Methyl-2-phenyl-2-((2S,4S,6R)-2,4,6-trimethyloctamido)-acetate (**13b**).* A solution of the remaining half-portion of the above material containing **12** (19.10 mg), HBTU (78.50 mg, 0.21 mmol), HOBt (33.0 mg, 0.24 mmol), DIEA (35.50 mL, 0.21 mmol), and (*S*)-PGME·HCl (44.80 mg, 0.22 mmol) in 1.0 mL of anhydrous DMF was stirred for 10 h at room temperature. The reaction mixture was quenched with saturated aqueous NH_4Cl, dried over anhydrous Na_2SO_4, and concentrated in vacuo. The residue was chromatographed (SiO_2, n-hexane/EtOAc 3/1) to yield **13b** (6.0 mg, 61% over two steps) as a colorless oil: $[\alpha]_D^{20}$ = +113.41° (c 0.50, $CHCl_3$); IR (neat) 3300, 2960, 2927, 1749, 1647 cm^{-1}; ^{1}H NMR ($CDCl_3$, 500 MHz) δ 7.30–7.37 (5H), 6.36 (NH), 5.59 (d, J = 7.4 Hz, 1H), 3.73 (s, 3H), 2.41 (m, 1H), 1.65 (ddd, J = 6.0, 8.5, 14.0 Hz, 1H), 1.54 (m, 1H), 1.39 (m, 1H), 1.25 (m, 1H), 1.17 (m, 1H), 1.14 (m, 1H), 1.11 (d, J = 6.4 Hz, 3H), 1.03 (m, 2H), 0.87 (d, J = 6.8 Hz, 3H), 0.85 (t, J = 7.2 Hz, 3H), 0.79 (d, J = 6.4 Hz, 3H); ^{13}C NMR ($CDCl_3$, 125 MHz) δ 175.9, 171.5, 136.7, 129.0, 128.7, 127.2, 56.1, 52.7, 44.3, 42.5, 38.2, 31.6, 30.4, 27.9, 19.6, 18.9, 18.3, 11.4; HRMS (ESI) m/z 356.2201 $[M + Na]^+$ calcd for $C_{20}H_{31}NNaO_3$, 356.2196.

PGME Derivatives of Synthetic (2*S*,4*S*,6*S*)-Trimethyloctanoic Acid (14a,b). *(S)-4-Benzyl-3-((2R,4S)-5-((4-methoxybenzyl)oxy)-2,4-dimethylpentanoyl)oxazolidin-2-one (**S1**).*

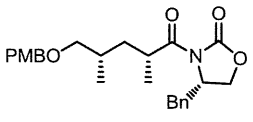

This compound was synthesized in the same manner as that of **8** (1.7 g, 53% over four steps). The ratio of **S1** and its diastereomer was 27:1, as judged from their yield: $[\alpha]_D^{20}$ = +21.49° (c 0.73, $CHCl_3$); IR (neat) 2957, 2931, 2854, 1775, 1694, 1207, 702 cm^{-1}; ^{1}H NMR ($CDCl_3$, 500 MHz) δ 6.84–7.34 (9H), 4.66 (m, 1H), 4.44 (s, 2H), 4.09–4.18 (m, 2H), 3.96 (m, 1H), 3.77 (s, 3H), 3.28 (dd, J = 3.2, 13.5 Hz, 1H), 3.41 (dd, J = 5.5, 8.7 Hz, 1H), 3.24 (dd, J = 6.7, 9.1 Hz, 1H), 2.67 (dd, J = 10.3, 13.9 Hz, 1H), 1.96 (ddd, J = 6.2, 7.5, 14.0 Hz, 1H),

1.86 (m, 1H), 1.25 (ddd, J = 6.3, 7.5, 13.6 Hz, 1H), 1.20 (d, J = 6.7 Hz, 3H), 1.0 (d, J = 6.7 Hz, 3H); ^{13}C NMR ($CDCl_3$, 125 MHz) δ 177.1, 158.9, 152.9, 135.3, 130.7, 129.2, 128.9, 128.8, 127.1, 113.6, 75.2, 72.4, 65.8, 55.2, 55.1, 37.9 (2C), 35.1, 31.3, 17.9, 17.6; HRMS (ESI) m/z 448.2119 $[M + Na]^+$ calcd for $C_{25}H_{31}NNaO_5$, 448.2094; colorless oil.

*(2R,4S)-5-((4-Methoxybenzyl)oxy)-2,4-dimethylpentan-1-ol (**S2**).*

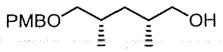

This compound was synthesized in the same manner as that of **9** (0.8 g, 87%): $[\alpha]_D^{20}$ = +5.73° (c 1.07, $CHCl_3$); IR (neat) 3405, 2910, 2869, 1512, 1246, 1035 cm^{-1}; ^{1}H NMR ($CDCl_3$, 500 MHz) δ 7.23 (d, J = 8.9 Hz, 2H), 6.85 (d, J = 8.9 Hz, 2H), 4.40 (d, J = 3.4 Hz, 2H), 3.75 (s, 3H), 3.40 (dd, J = 5.3, 10.8 Hz, 1H), 3.31 (dd, J = 5.8, 10.3 Hz, 1H), 3.28 (dd, J = 5.8, 8.9 Hz, 1H), 3.19 (dd, J = 6.4, 9.7 Hz, 1H), 1.83 (m, 1H), 1.66 (m, 1H), 1.45 (m, 1H), 0.93 (d, J = 7.5 Hz, 3H), 0.91 (d, J = 6.9 Hz, 3H), 0.90 (m, 1H); ^{13}C NMR ($CDCl_3$, 125 MHz) δ 158.8, 130.4, 128.9, 113.5, 75.4, 72.4, 67.3, 54.9, 37.4, 32.9, 30.7, 17.9, 17.4; HRMS (ESI) m/z 275.1616 $[M + Na]^+$ calcd for $C_{15}H_{24}NaO_3$, 275.1618; colorless oil.

*1-((((2S,4S)-2,4-Dimethylhexyl)oxy)methyl)-4-methoxybenzene (**S3**).*

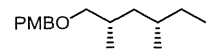

This compound was synthesized in the same manner as that of **10** (0.6 g, 75% over two steps): $[\alpha]_D^{20}$ = +12.06° (c 0.84, $CHCl_3$); IR (neat) 2956, 2910, 1511, 1245, 1095, 819 cm^{-1}; ^{1}H NMR ($CDCl_3$, 500 MHz) δ 7.30 (d, J = 8.3 Hz, 2H), 6.91 (d, J = 9.5 Hz, 2H), 4.47 (d, J = 7.6 Hz, 2H), 3.82 (s, 3H), 3.37 (dd, J = 7.2, 9.2 Hz, 1H), 3.22 (dd, J = 5.3, 9.1 Hz, 1H), 1.90 (m, 1H), 1.47 (m, 1H), 1.40 (m, 1H), 1.39 (m, 1H), 1.14 (m, 1H), 0.99 (d, J = 6.7 Hz, 3H), 0.97 (m, 1H), 0.92 (d, J = 6.7 Hz, 3H), 0.91 (t, J = 6.7 Hz, 3H); ^{13}C NMR ($CDCl_3$, 125 MHz) δ 158.9, 130.9, 128.9, 113.6, 75.7, 72.5, 55.0, 41.1, 31.5, 30.8, 29.0, 19.7, 17.9, 11.1; HRMS (ESI) m/z 273.1823 $[M + Na]^+$ calcd for $C_{16}H_{26}NaO_2$, 273.1825; colorless oil.

*(R)-4-Benzyl-3-((2S,4S,6S)-2,4,6-trimethyloctanoyl)oxazolidin-2-one (**S4**).*

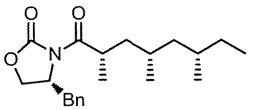

This compound was synthesized in the same manner as that of **11** (41.2 mg, 11% over three steps). The ratio of **S4** and its diastereomer was 54:1, as judged from their yield: $[\alpha]_D^{20}$ = −20.58° (c 0.83, $CHCl_3$); IR (neat) 2957, 2913, 1778, 1696, 1383, 1204 cm^{-1}; ^{1}H NMR ($CDCl_3$, 500 MHz) δ 7.20–7.35 (5H), 4.69 (m, 1H), 4.16 (m, 2H), 3.97 (m, 1H), 3.30 (dd, J = 3.5, 13.8 Hz, 1H), 2.73 (dd, J = 9.8, 13.3 Hz, 1H), 1.92 (ddd, J = 5.1, 9.0, 13.7 Hz, 1H), 1.71 (d, J = 6.8 Hz, 3H), 1.51 (m, 1H), 1.47 (m, 1H), 1.34 (m, 1H), 1.26 (m, 1H), 1.11 (m, 1H), 1.08 (m, 1H), 0.94 (m, 1H), 0.92 (d, J = 7.1 Hz, 3H), 0.86 (t, J = 7.8 Hz, 3H), 0.85 (d, J = 7.0 Hz, 3H); ^{13}C NMR ($CDCl_3$, 125 MHz) δ 177.6, 153.0, 135.3, 129.4, 128.9, 127.3, 65.8, 55.3, 44.5, 41.3, 38.0, 35.1, 31.4, 29.0, 28.3, 20.6, 19.6, 18.2, 11.1; HRMS (ESI) m/z 368.2197 $[M + Na]^+$ calcd for $C_{21}H_{31}NNaO_3$, 368.2196; colorless oil.

*(R)-Methyl 2-Phenyl-2-((2S,4S,6S)-2,4,6-trimethyloctamido)-acetate (**14a**).*

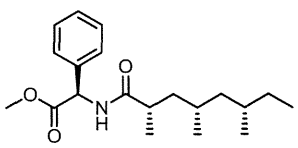

This compound was synthesized in the same manner as that of **13a** (8.08 mg, 86% over two steps): $[\alpha]_D^{20}$ = −102.90° (c 0.81, $CHCl_3$); IR (neat) 3293, 2956, 2926, 1746, 1648 cm^{-1}; ^{1}H NMR ($CDCl_3$, 500 MHz) δ 7.29–7.36 (5H), 6.42 (NH), 5.60 (d, J = 7.3 Hz, 1H), 3.73 (s, 3H), 2.39 (m, 1H), 1.68 (ddd, J = 4.6, 9.7, 14.0 Hz, 1H), 1.34 (m, 2H), 1.22 (m, 1H), 1.15 (d, J = 6.7 Hz, 3H), 1.10 (m, 1H), 1.02 (m, 1H), 0.95 (m, 1H), 0.85 (m, 1H), 0.83 (d, J = 6.7 Hz, 3H), 0.79 (t, J = 7.5 Hz, 3H), 0.70 (d, J = 6.6 Hz, 3H); ^{13}C NMR ($CDCl_3$, 125 MHz) δ 175.8, 171.6, 136.8, 128.9, 128.4, 127.2, 56.1, 52.7, 44.9, 41.9, 38.9, 31.3, 28.0, 29.0, 20.2, 19.5, 18.6, 11.2; HRMS (ESI) m/z 356.2199 $[M + Na]^+$ calcd for $C_{20}H_{31}NNaO_3$, 356.2196; colorless oil.

*(S)-Methyl 2-Phenyl-2-((2S,4S,6S)-2,4,6-trimethyloctamido)-acetate (**14b**).*

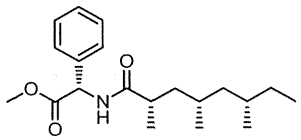

This compound was synthesized in the same manner as that of **13b** (9.2 mg, 91% over two steps): $[\alpha]_D^{20}$ = 114.56° (c 0.92, $CHCl_3$); IR (neat) 3296, 2957, 2927, 1748, 1645, 697 cm^{-1}; ^{1}H NMR ($CDCl_3$, 500 MHz) δ 7.30–7.37 (5H), 6.36 (NH), 5.59 (d, J = 7.3 Hz, 1H), 3.73 (s, 3H), 2.41 (m, 1H), 1.72 (ddd, J = 4.8, 9.5, 14.1 Hz, 1H), 1.53 (m, 1H), 1.41 (m, 1H), 1.32 (m, 1H), 1.12 (d, J = 6.5 Hz, 3H), 1.17 (m, 1H), 1.05 (m, 1H), 1.04 (m, 1H), 0.92 (m, 1H), 0.89 (d, J = 7.0 Hz, 3H), 0.84 (t, J = 7.4 Hz, 3H), 0.80 (d, J = 6.7 Hz, 3H); ^{13}C NMR ($CDCl_3$, 125 MHz) δ 175.8, 171.5, 136.7, 129.0, 128.4, 127.2, 56.2, 52.7, 45.0, 41.7, 38.9, 31.5, 29.1, 28.0, 20.3, 19.7, 18.7, 11.2; HRMS (ESI) m/z 356.2204 $[M + Na]^+$ calcd for $C_{20}H_{31}NNaO_3$, 356.2196; colorless oil.

PGME Derivatives of Synthetic (2*S*,4*R*,6*R*)-Trimethyloctanoic acid (15a,b). *(R)-4-Benzyl-3-((2S,4R)-5-((4-methoxybenzyl)oxy)-2,4-dimethylpentanoyl)oxazolidin-2-one (**S5**).*

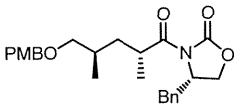

This compound was synthesized in the same manner as that of **8** (1.7 g, 33% over four steps). The ratio of **S5** and its diastereomer was 10:1, as judged from their yield: $[\alpha]_D^{20}$ = +7.02° (c 0.71, $CHCl_3$); IR (neat) 2976, 2934, 2857, 1776, 1695, 1206, 1093, 701 cm^{-1}; ^{1}H NMR ($CDCl_3$, 500 MHz) δ 6.86–7.33 (9H), 4.62 (m, 1H), 4.42 (s, 2H), 4.13 (m, 1H), 4.06 (dd, J = 3.0, 9.1 Hz, 1H), 3.89 (m, 1H), 3.79 (s, 3H), 3.25 (dd, J = 3.2, 13.4 Hz, 1H), 3.30 (m, 2H), 2.51 (dd, J = 10.2, 13.2 Hz, 1H), 1.89 (m, 1H), 1.67 (ddd, J = 7.0, 8.0, 14.6 Hz, 1H), 1.52 (ddd, J = 6.4, 7.5, 13.8 Hz, 1H), 1.16 (d, J = 7.0 Hz, 3H), 0.97 (d, J = 6.8 Hz, 3H); ^{13}C NMR ($CDCl_3$, 125 MHz) δ 177.3, 159.0, 152.9, 135.5, 130.7, 129.9 (2C), 113.6, 128.8, 127.1, 75.8, 72.7, 65.8, 55.6 (2C), 37.9, 37.8, 35.2, 31.2, 17.0 (2C); HRMS (ESI) m/z 448.2115 $[M + Na]^+$ calcd for $C_{25}H_{31}NNaO_5$, 448.2094; colorless oil.

*(2S,4R)-5-((4-Methoxybenzyl)oxy)-2,4-dimethylpentan-1-ol (**S6**).*

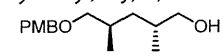

This compound was synthesized in the same manner as that of **9** (0.7 g, 77%): $[\alpha]_D^{20}$ = +15.03° (c 0.92, $CHCl_3$); IR (neat) 3405, 2912, 2869, 1512, 1244, 1033, 819 cm^{-1}; ^{1}H NMR ($CDCl_3$, 500 MHz) δ 7.24 (d, J = 8.3rrr Hz, 2H), 6.86 (d, J = 8.6 Hz, 2H), 4.42 (s, 2H), 3.77 (s, 3H), 3.41 (dd, J = 6.5, 10.5 Hz, 1H), 3.36 (dd, J = 6.3, 10.5 Hz, 1H), 3.27 (dd, J = 6.3, 8.8 Hz, 1H), 3.23 (dd, J = 6.9, 9.2 Hz, 1H), 1.87 (m, 1H), 1.71 (m, 1H), 1.18 (m, 2H), 0.89 (d, J = 6.6 Hz, 3H), 0.87 (d, J = 6.8 Hz, 3H); ^{13}C NMR ($CDCl_3$, 125 MHz) δ 158.9, 139.0, 130.5, 113.5, 76.0, 72.5, 68.4, 55.0, 37.0, 32.8, 30.4, 16.8, 16.2; HRMS (ESI) m/z 275.1616 $[M + Na]^+$ calcd for $C_{15}H_{24}NaO_3$, 275.1618; colorless oil.

*1-((((2R,4R)-2,4-Dimethylhexyl)oxy)methyl)-4-methoxybenzene (**S7**).*

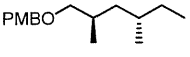

This compound was synthesized in the same manner as that of **10** (0.6 g, 96% over two steps): $[\alpha]_D^{20}$ = +12.09° (c 0.82, $CHCl_3$), IR (neat) 2956, 2910, 2850, 1511, 1246, 1096, 820 cm^{-1}; ^{1}H NMR ($CDCl_3$, 500 MHz) δ 7.31 (d, J = 8.4 Hz, 2H), 6.92 (d, J = 8.9 Hz, 2H), 4.49 (d, J = 2.5 Hz, 2H), 3.81 (s, 3H), 3.35 (dd, J = 5.8, 8.9 Hz, 1H), 3.25 (dd, J = 7.1, 8.9 Hz, 1H), 1.92 (m, 1H), 1.48 (m, 1H), 1.38 (m, 1H), 1.23 (m, 2H), 1.16 (m, 1H), 0.97 (d, J = 6.7 Hz, 3H), 0.94 (t, J = 7.4 Hz, 3H), 0.91 (d, J = 6.5 Hz, 3H); ^{13}C NMR ($CDCl_3$, 125 MHz) δ 158.9, 130.8, 128.9, 113.6, 76.3, 72.4, 55.0, 40.6, 31.5, 30.8, 30.3, 18.8, 16.9, 11.3; IR

dx.doi.org/10.1021/jo500906v | J. Org. Chem. 2014, 79, 6858–6867

(neat) 2956, 2910, 2810, 1511, 1245, 1096, 819 cm^{-1}; ^1H NMR ($CDCl_3$, 500 MHz); HRMS (ESI) *m/z* 273.1823 $[M + Na]^+$ calcd for $C_{16}H_{26}NaO_2$, 273.1825; colorless oil.

*(R)-4-Benzyl-3-((2S,4R,6R)-2,4,6-trimethyloctanoyl)oxazolidin-2-one (**S8**).*

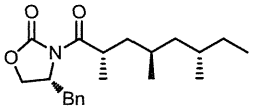

This compound was synthesized in the same manner as that of **11** (36.3 mg, 16% over 3 steps). The ratio of **S8** and its diastereomer was 3:1, as judged from their yield: $[\alpha]_D^{20} = -15.79°$ (*c* 0.94, $CHCl_3$); IR (neat) 2960, 2916, 1780, 1698, 1383, 1209 cm^{-1}; ^1H NMR ($CDCl_3$, 500 MHz) δ 7.20–7.35 (5H), 4.68 (m, 1H), 4.16 (m, 2H), 3.89 (m, 1H), 3.32 (dd, *J* = 3.6, 13.9 Hz, 1H), 2.69 (dd, *J* = 10.1, 13.0 Hz, 1H), 1.63 (m, 1H), 1.59 (m, 1H), 1.41 (m, 1H), 1.35 (m, 1H), 1.29 (m, 1H), 1.16 (m, 1H/d, *J* = 7.0 Hz, 3H), 1.10 (m, 2H), 0.89 (d, *J* = 5.8 Hz, 3H), 0.87 (t, *J* = 7.3 Hz, 3H), 0.83 (d, *J* = 6.7 Hz, 3H); ^{13}C NMR ($CDCl_3$, 125 MHz) δ 177.8, 153.0, 135.5, 129.4, 128.9, 127.3, 65.9, 55.4, 44.7, 41.7, 38.1, 35.3, 31.6, 30.2, 27.9, 19.0 (2C), 16.8, 11.4; HRMS (ESI) *m/z* 368.2198 $[M + Na]^+$ calcd for $C_{21}H_{31}NNaO_3$, 368.2196; colorless oil.

*(R)-Methyl 2-Phenyl-2-((2S,4R,6R)-2,4,6-trimethyloctamido)-acetate (**15a**).*

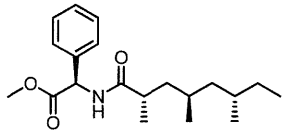

This compound was synthesized in the same manner as that of **13a** (8.0 mg, 82% over two steps): $[\alpha]_D^{20} = -82.39°$ (*c* 0.74, $CHCl_3$); IR (neat) 3282, 2959, 2920, 1751, 1634 cm^{-1}; ^1H NMR ($CDCl_3$, 500 MHz) δ 7.29–7.36 (5H), 6.38 (NH), 5.60 (d, *J* = 7.8 Hz, 1H), 3.73 (s, 3H), 2.38 (m, 1H), 1.50 (m, 1H), 1.46 (m, 1H), 1.35 (m. 1H), 1.27 (m, 1H), 1.23 (m, 1H), 1.15 (d, *J* = 6.7 Hz, 3H), 1.02 (m, 2H), 0.96 (m, 1H), 0.83 (t, *J* = 7.7 Hz, 3H), 0.77 (d, *J* = 6.5 Hz, 3H), 0.70 (d, *J* = 6.7 Hz, 3H); ^{13}C NMR ($CDCl_3$, 125 MHz) δ 176.1, 171.6, 136.7, 128.9, 128.4, 128.3, 56.2, 52.8, 44.4, 42.3, 38.8, 31.6, 30.4, 27.8, 19.4, 18.8, 17.8, 11.4; HRMS (ESI) *m/z* 356.2200 $[M + Na]^+$ calcd for $C_{20}H_{31}NNaO_3$, 356.2196; colorless amorphous solid.

*(S)-Methyl 2-Phenyl-2-((2S,4R,6R)-2,4,6-trimethyloctamido)-acetate (**15b**).*

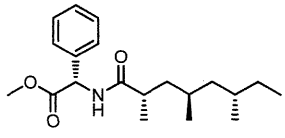

This compound was synthesized in the same manner as that of **13b** (8.5 mg, 88% over two steps): $[\alpha]_D^{20} = +128.66°$ (*c* 0.73, $CHCl_3$); IR (neat) 3295, 2959, 2926, 1748, 1647 cm^{-1}; ^1H NMR ($CDCl_3$, 500 MHz) δ 7.23–7.37 (5H), 6.38 (NH), 5.58 (d, *J* = 6.5 Hz, 1H), 3.73 (s, 3H), 2.38 (m, 1H), 1.54 (m, 1H), 1.53 (m, 1H), 1.40 (m, 1H), 1.31 (m, 1H), 1.27 (m, 1H), 1.14 (m, 1H), 1.10 (d, *J* = 7.0 Hz, 3H), 1.08 (m, 2H), 0.86 (t, *J* = 7.4 Hz, 3H), 0.83 (d, *J* = 6.6 Hz, 3H), 0.81 (d, *J* = 7.0 Hz, 3H); ^{13}C NMR ($CDCl_3$, 125 MHz) δ 176.1, 171.5, 136.8, 128.9, 128.5, 127.2, 56.2, 52.7, 44.5, 42.4, 38.8, 31.7, 30.4, 27.8, 19.4, 18.9, 17.6, 11.4; HRMS (ESI) *m/z* 356.2195 $[M + Na]^+$ calcd for $C_{20}H_{31}NNaO_3$, 356.2196; colorless oil.

PGME Derivatives of Synthetic (2S,4R,6S)-Trimethyloctanoic Acid (16a,b). *(S)-4-Benzyl-3-((2R,4R)-5-((4-methoxybenzyl)oxy)-2,4-dimethylpentanoyl)oxazolidin-2-one (**S9**).*

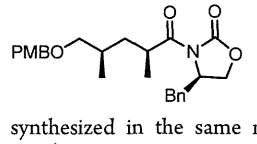

This compound was synthesized in the same manner as that of **8** (1.9 g, 32% over four steps). The ratio of **S9** and its diastereomer was 23:1, as judged from their yield: $[\alpha]_D^{20} = -21.85°$ (*c* 0.93, $CHCl_3$); IR (neat) 2958, 2931, 2854, 1775, 1695, 1385, 1207, 1092, 819, 702 cm^{-1}; ^1H NMR ($CDCl_3$, 500 MHz) δ 6.85–7.35 (9H), 4.67 (m, 1H), 4.45 (s, 2H), 4.11–4.19 (m, 2H), 3.96 (m, 1H), 3.41 (dd, *J* = 5.8, 9.5 Hz, 1H), 3.29 (dd, *J* = 3.5, 13.2 Hz, 1H), 3.24 (dd, *J* = 7.0, 9.3 Hz, 1H), 2.67 (dd, *J* = 9.7, 13.2 Hz, 1H), 1.97 (ddd, *J* = 6.2, 8.2, 14.1 Hz, 1H), 1.86 (m, 1H), 1.25 (ddd, *J* = 6.4, 7.5, 13.6 Hz, 1H), 1.20 (d, *J* = 6.8 Hz, 3H), 1.00 (d, *J* = 6.6 Hz, 3H); ^{13}C NMR ($CDCl_3$, 125 MHz) δ 177.2, 158.9, 153.0, 135.3, 130.8, 129.3, 129.0, 128.8, 127.2, 113.6, 75.2, 72.5, 65.8, 55.3, 55.1, 38.0, 37.9, 35.1, 31.3, 18.0, 17.7; HRMS (ESI) *m/z* 448.2106 $[M + Na]^+$ calcd for $C_{25}H_{31}NNaO_5$, 448.2094; colorless oil.

*(2R,4R)-5-((4-Methoxybenzyl)oxy)-2,4-dimethylpentan-1-ol (**S10**).*

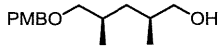

This compound was synthesized in the same manner as that of **9** (0.8 g, 85%): $[\alpha]_D^{20} = -5.22°$ (*c* 1.05, $CHCl_3$); IR (neat) 3362, 2911, 2869, 1511, 1246, 1033, 822 cm^{-1}; ^1H NMR ($CDCl_3$, 500 MHz) δ 7.23 (d, *J* = 9.2 Hz, 2H), 6.85 (d, *J* = 8.3 Hz, 2H), 4.40 (d, *J* = 3.5 Hz, 2H), 3.75 (s, 3H), 3.40 (dd, *J* = 5.3, 10.2 Hz, 1H), 3.31 (dd, *J* = 6.2, 10.5 Hz, 1H), 3.28 (dd, *J* = 6.0, 9.1 Hz, 1H), 3.19 (dd, *J* = 7.1, 9.4 Hz, 1H), 1.83 (m, 1H), 1.66 (m, 1H), 1.45 (m, 1H), 0.93 (d, *J* = 6.9 Hz, 3H), 0.91 (d, *J* = 6.4 Hz, 3H), 0.90 (m, 1H); ^{13}C NMR ($CDCl_3$, 125 MHz) δ 158.9, 130.4, 128.9, 113.5, 75.4, 72.5, 67.3, 54.9, 37.5, 32.9, 30.7, 17.9, 17.4; HRMS (ESI) *m/z* 275.1613 $[M + Na]^+$ calcd for $C_{15}H_{24}NaO_3$, 275.1618; colorless oil.

*1-((((2R,4S)-2,4-Dimethylhexyl)oxy)methyl)-4-methoxybenzene (**S11**).*

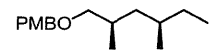

This compound was synthesized in the same manner as that of **10** (0.6 g, 76% over two steps): $[\alpha]_D^{20} = -10.43°$ (*c* 1.21, $CHCl_3$); IR (neat) 2910, 2851, 1512, 1245, 1095, 819 cm^{-1}; ^1H NMR ($CDCl_3$, 500 MHz) δ 7.30 (d, *J* = 8.3 Hz, 2H), 6.91 (d, *J* = 8.7 Hz, 2H), 4.67 (d, *J* = 7.6 Hz, 2H), 3.82 (s, 3H), 3.36 (dd, *J* = 5.5, 9.0 Hz, 1H), 3.21 (dd, *J* = 7.3, 9.3 Hz, 1H), 1.89 (m, 1H), 1.46 (m, 1H), 1.40 (m, 1H), 1.38 (m, 1H), 1.13 (m, 1H), 0.98 (d, *J* = 6.9 Hz, 3H), 0.97 (m, 1H), 0.91 (d, *J* = 6.3 Hz, 3H/t, *J* = 6.3 Hz, 3H); ^{13}C NMR ($CDCl_3$, 125 MHz) δ 159.0, 130.9, 128.9, 113.6, 75.7, 72.5, 55.0, 41.1, 31.5, 30.9, 29.0, 19.7, 18.0, 11.1; HRMS (ESI) *m/z* 273.1821 $[M + Na]^+$ calcd for $C_{16}H_{26}NaO_2$, 273.1825; colorless oil.

*(R)-4-Benzyl-3-((2S,4R,6S)-2,4,6-trimethyloctanoyl)oxazolidin-2-one (**S12**).*

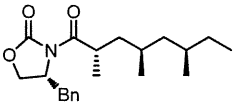

This compound was synthesized in the same manner as that of **11** (39.4 mg, 15% over three steps). The ratio of **S12** and its diastereomer was 4:1, as judged from their yield: $[\alpha]_D^{20} = -41.31°$ (*c* 0.75, $CHCl_3$); IR (neat) 2959, 2915, 1779, 1697, 1209 cm^{-1}; ^1H NMR ($CDCl_3$, 500 MHz) δ 7.20–7.34 (5H), 4.67 (m, 1H), 3.85 (m, 1H), 3.30 (dd, *J* = 2.8, 13.7 Hz, 1H), 2.70 (dd, *J* = 10.0, 13.5 Hz, 1H), 1.61 (m, 1H), 1.52 (m, 1H), 1.43 (m, 1H), 1.42 (m, 1H), 1.34 (m, 1H), 1.24 (m, 1H), 1.15 (d, *J* = 7.0 Hz, 3H), 1.08 (m, 1H), 0.99 (m, 1H), 0.91 (d, *J* = 6.4 Hz, 3H), 0.86 (t, *J* = 6.7 Hz, 3H), 0.85 (d, *J* = 6.7 Hz, 3H); ^{13}C NMR ($CDCl_3$, 125 MHz) δ 177.8, 152.9, 135.4, 129.4, 128.9, 127.3, 65.9, 55.3, 45.1, 40.6, 38.0, 35.3, 31.5, 29.2, 27.7, 19.7, 19.5, 16.4, 11.2; HRMS (ESI) *m/z* 368.2198 $[M + Na]^+$ calcd for $C_{21}H_{31}NNaO_3$, 368.2196; colorless oil.

*(R)-Methyl 2-Phenyl-2-((2S,4R,6S)-2,4,6-trimethyloctamido)-acetate (**16a**).*

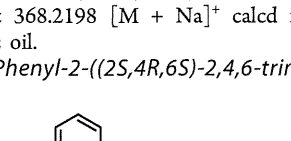

This compound was synthesized in the same manner as that of **13a** (10.7 mg, 87% over two steps): $[\alpha]_D^{20} = -117.43°$ (*c* 0.89, $CHCl_3$); IR (neat) 3275, 2959, 2915, 1752, 1641, 1535 cm^{-1}; ^1H NMR

dx.doi.org/10.1021/jo500906v | J. Org. Chem. 2014, 79, 6858–6867

($CDCl_3$, 500 MHz) δ 7.30–7.37 (5H), 6.40 (NH), 5.60 (d, J = 8.1 Hz, 1H), 3.73 (s, 3H), 2.36 (m, 1H), 1.48 (m, 1H), 1.38 (m, 2H), 1.37 (m, 1H), 1.26 (m, 1H), 1.17 (m, 1H), 1.14 (d, J = 7.0 Hz, 3H), 0.97 (m, 1H), 0.90 (m, 1H), 0.80 (m, 3H), 0.79 (m, 3H) 0.78 (m, 3H); ^{13}C NMR ($CDCl_3$, 125 MHz) δ 176.2, 171.6, 136.7, 129.0, 128.5, 127.3, 56.2, 52.7, 44.9, 41.3, 38.7, 31.4, 29.0, 27.8, 20.1, 19.7, 17.5, 11.2; HRMS (ESI) m/z 356.2205 $[M + Na]^+$ calcd for $C_{20}H_{31}NNaO_3$, 356.2196; colorless oil.

(S)-Methyl 2-Phenyl-2-((2S,4R,6S)-2,4,6-trimethyloctamido)-acetate (16b).

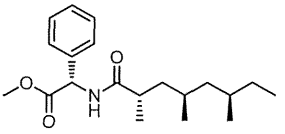

This compound was synthesized in the same manner as that of **13a** (11.3 mg, 92% over two steps): $[\alpha]_D^{20}$ = +104.87° (c 0.94, $CHCl_3$); IR (neat) 3307, 2958, 2928, 1749, 1649, 1524 cm^{-1}; ^1H NMR ($CDCl_3$, 500 MHz) δ 7.30–7.37 (5H), 6.39 (NH), 5.57 (d, J = 6.9 Hz, 1H), 3.73 (s, 3H), 2.37 (m, 1H), 1.55 (m, 1H), 1.43 (m, 1H), 1.42 (m, 2H), 1.34 (m, 1H), 1.23 (m, 1H), 1.10 (d, J = 6.8 Hz, 3H), 1.05 (m, 1H), 0.95 (m, 1H), 0.85 (m, 6H), 0.84 (m, 3H); ^{13}C NMR ($CDCl_3$, 125 MHz) δ 176.1, 171.5, 136.7, 128.9, 128.5, 127.2, 56.2, 52.7, 44.5, 42.1, 38.8, 31.6, 30.4, 27.8, 20.9, 19.4, 17.6, 11.4; HRMS (ESI) m/z 356.2203 $[M + Na]^+$ calcd for $C_{20}H_{31}NNaO_3$, 356.2196; colorless oil.

■ ASSOCIATED CONTENT

Supporting Information

Text, a table, and figures giving ^1H and ^{13}C NMR spectra of synthesized materials and natural product derivatives and a list of analyzed compounds. This material is available free of charge via the Internet at http://pubs.acs.org.

■ AUTHOR INFORMATION

Corresponding Author

*E-mail for H.K.: scseigyo-hisyo@pharm.kyoto-u.ac.jp.

Notes

The authors declare no competing financial interest.

■ ACKNOWLEDGMENTS

This work was supported in part by research grants from the Japan Society for the Promotion of Sciences (JSPS), the Ministry of Health and Welfare of Japan, and the Ministry of Education, Culture, Sports, Science and Technology (MEXT) of Japan.

■ REFERENCES

(1) Feher, M.; Schmidt, J. M. *J. Chem. Inf. Comput. Sci.* **2003**, *43*, 218.
(2) Newman, D. J.; Cragg, G. M. *J. Nat. Prod.* **2012**, *75*, 311.
(3) Bifulco, G.; Dambruoso, P.; Gomez-Paloma, L.; Riccio, R. *Chem. Rev.* **2007**, *107*, 3744.
(4) Matsumori, N.; Kaneno, D.; Murata, M.; Nakamura, H.; Tachibana, K. *J. Org. Chem.* **1999**, *64*, 866.
(5) Murata, M.; Matsuoka, S.; Matsumori, N.; Paul, G. K.; Tachibana, K. *J. Am. Chem. Soc.* **1999**, *121*, 870.
(6) Lee, J.; Kobayashi, Y.; Tezuka, K.; Kishi, Y. *Org. Lett.* **1999**, *1*, 2181.
(7) Kobayashi, Y.; Lee, J.; Tezuka, K.; Kishi, Y. *Org. Lett.* **1999**, *1*, 2177.
(8) Higashibayashi, S.; Czechtizky, W.; Kobayashi, Y.; Kishi, Y. *J. Am. Chem. Soc.* **2003**, *125*, 14379.
(9) Akiyama, K.; Kawamoto, S.; Fujimoto, H.; Ishibashi, M. *Tetrahedron Lett.* **2003**, *44*, 8427.
(10) Schmidt, Y.; Breit, B. *Org. Lett.* **2010**, *12*, 2218.
(11) Schmidt, Y.; Lehr, K.; Colas, L.; Breit, B. *Chem. Eur. J.* **2012**, *18*, 7071.
(12) Stahl, M.; Schopfer, U.; Frenking, G.; Hoffmann, R. W. *J. Org. Chem.* **1996**, *61*, 8083.
(13) Kishimoto, S.; Tsunematsu, Y.; Nishimura, S.; Hayashi, Y.; Hattori, A.; Kakeya, H. *Tetrahedron* **2012**, *68*, 5572.
(14) Motohashi, K.; Toda, T.; Sue, M.; Furihata, K.; Shizuri, Y.; Matsuo, Y.; Kasai, H.; Shin-Ya, K.; Takagi, M.; Izumikawa, M.; Horikawa, Y.; Seto, H. *J. Antibiot.* **2010**, *63*, 549.
(15) Nishiyama, Y.; Sugawara, K.; Tomita, K.; Yamamoto, H.; Kamei, H.; Oki, T. *J. Antibiot.* **1993**, *46*, 921.
(16) Sugawara, K.; Toda, S.; Moriyama, T.; Konishi, M.; Oki, T. *J. Antibiot.* **1993**, *46*, 928.
(17) Reduction using $NaBH_4$ gave two diastereomers, compound **4** and its epimer at C24. The ratio of compound **4** and its diastereomer was 2.5:1.
(18) Stahl, M.; Schopfer, U.; Frenking, G.; Hoffmann, R. W. *Mol. Phys.* **1997**, *92*, 569.
(19) Evans, D. A.; Dow, R. L.; Shih, T. L.; Takacs, J. M.; Zahler, R. *J. Am. Chem. Soc.* **1990**, *112*, 5290.
(20) The ratio of compound **8** and its diastereomer was 10.6:1. The absolute stereochemistry at the β position in these compounds was confirmed by analyzing PGME derivatives of the hydrolyzed products.
(21) Xaio, J.; Kumazawa, S.; Yoshikawa, N.; Mikawa, T.; Sato, Y. *J. Antibiot.* **1993**, *46*, 48.
(22) Lin, Z.; Flores, M.; Forteza, I.; Henriksen, N. M.; Concepcion, G. P.; Rosenberg, G.; Haygood, M. G.; Olivera, B. M.; Light, A. R.; Cheatham, T. E., 3rd; Schmidt, E. W. *J. Nat. Prod.* **2012**, *75*, 644.
(23) Tsantrizos, Y. S.; Shen, J. H.; Trimble, L. A. *Tetrahedron Lett.* **1997**, *38*, 7033.

参考資料

厚生労働科学研究費補助金
肝炎等克服実用化研究事業
B型肝炎創薬実用化等研究事業

「次世代生命基盤技術を用いたB型肝炎制圧のための創薬研究」（第5回班会議）
理化学研究所　小嶋聡一

「B型肝炎ウイルス構造解析による薬剤応答性の評価と新規治療薬開発に関する研究」
大阪市立大学　村上善基

「エクソソームを介したＨＢＶ感染及び発がんメカニズム解析と治療戦略」
国立がん研究センター研究所　落谷孝広

合同班会議　要旨集

平成26年7月26日（土）～27日（日）

国立感染症研究所　戸山庁舎　第一会議室

世話人　国立感染症研究所　相崎英樹